submitted to *J. Chem. Phys.*

# Thermochemistry and Mechanisms of the $Pt^+ + SO_2$ Reaction from Guided Ion Beam Tandem Mass Spectrometry and Theory

P. B. Armentrout

*Department of Chemistry, University of Utah, 315 S 1400 E Rm 2020, Salt Lake City, UT 84112, United States of America*

## ABSTRACT

The kinetic energy dependences of the reactions of $Pt^+$ ($^2D_{5/2}$) with $SO_2$ were studied using a guided ion beam tandem mass spectrometer and theory. Observed cationic products are $PtO^+$ and $PtSO^+$, with small amounts of $PtS^+$, all formed in endothermic reactions. Modeling the kinetic energy dependent product cross sections allows determination of the product bond dissociation energies (BDEs): $D_0(Pt^+\text{-}O) = 3.14 \pm 0.11$ eV, $D_0(Pt^+\text{-}S) = 3.68 \pm 0.31$ eV, and $D_0(Pt^+\text{-}SO) = 3.03 \pm 0.12$ eV. The oxide BDE agrees well with more precise literature values whereas the latter two results are the first such measurements. Quantum mechanical calculations were performed for $PtO^+$, $PtS^+$, $PtO_2^+$, and $PtSO^+$ at the B3LYP and coupled cluster with single, double, and perturbative triple [CCSD(T)] levels of theory using the def2-XZVPPD (X = T, Q) and aug-cc-pVXZ (X = T, Q, 5) basis sets and complete basis set (CBS) extrapolations. These theoretical BDEs agree well with the experimental values. After including empirical spin-orbit corrections, the product ground states are determined as $PtO^+$ ($^4\Sigma_{3/2}$), $PtS^+$ ($^4\Sigma_{3/2}$), $PtO_2^+$ ($^2\Sigma_g^+$), and $PtSO^+$ ($^2A'$). Potential energy profiles including intermediates and transition states for each reaction were also calculated at the B3LYP/def2-TZVPPD level. Periodic trends in the thermochemistry of the group 9 metal chalcogenide cations are compared, and the formation of $PtO^+$ from the $Pt^+ + SO_2$ reaction is compared with those from the $Pt^+ + O_2$, $CO_2$, CO, and NO reactions.

Corresponding author: armentrout@chem.utah.edu

## INTRODUCTION

Sulfur dioxide is released into the atmosphere by the combustion of fossil fuels and volcanic activity. In abundance, this substance is toxic[1, 2] and a major cause of acid rain.[3] Remediation of sulfur dioxide is therefore of great interest[4, 5] and has been achieved using a direct sulfur recovery process (DSRP).[6, 7] Transition metal complexes are potentially a viable means of catalytically reducing $SO_2$.[8-10] Therefore, a better understanding of $SO_2$ activation by transition metal systems would be valuable to advance such processes.

In the gas phase, oxidation of $SO_2$ by cerium and neutral vanadium oxide[11] and cationic cerium oxide[12] clusters has been examined. A recent study has observed that $Sc^+$ and $ScO^+$ activate $SO_2$ at thermal energies.[13] It can be anticipated that many early transition metal cations, which have strong metal-oxide bond energies, will react similarly. Further, we have recently shown that $Re^+$, $Os^+$, and $Ir^+$ can activate the OS-O bond but under endothermic conditions.[14-16] In these studies, we examined the kinetic energy dependences of these reactions using a guided ion beam tandem mass spectrometer (GIBMS). We also compared the oxidation reaction observed with prior work concerning reactions of these metal cations with $O_2$ and CO to help elucidate periodic trends and explain the origins of two endothermic features observed in the endothermic reactions of these three metal cations with $O_2$.[17-19] In contrast, the early metals, $Hf^+$, $Ta^+$, and $W^+$, react exothermically with $O_2$,[20] and $Pt^+$ and $Au^+$ exhibited only one endothermic feature in their kinetic energy dependent cross sections.[21, 22] Previously, we have examined the thermochemistry of $PtO^+$ by examining the endothermic reactions of $Pt^+$ with $O_2$, CO, and $CO_2$, obtaining an average bond dissociation energy (BDE) of 3.26 ± 0.07 eV.[21] The thermochemistry of $PtO_2^+$ was explored by studying endothermic reactions of $PtO^+$ with $O_2$ and $CO_2$ and collision-induced dissociation (CID) of $PtO_2^+$ with Xe and Ar.[23] Here, $PtO_2^+$ was generated both from sequential reactions with $N_2O$ and by complexation of $O_2$ with $Pt^+$. These two species exhibited distinct CID behavior as a function of kinetic energy, thereby allowing BDEs for loss of $O_2$ from the inserted $OPtO^+$ species and the $Pt^+(O_2)$ adduct to be independently ascertained as 1.20 ± 0.10 and 0.67 ± 0.05 eV, respectively.

In addition to the oxidation reactions, formation of $MO^+ + SO$, the reactions of $M^+ + SO_2$ ($M^+ = Re^+$, $Os^+$, and $Ir^+$) also provided thermochemistry for $MSO^+$, $MS^+$, and $MO_2^+$. The current study extends this research by examining reactions of $Pt^+$ with $SO_2$. Formation of the $PtO^+$ product competes with formation of $PtSO^+$ and small amounts of $PtO_2^+/PtS^+$ (which are isobaric at the resolution of the present study). Modeling the kinetic energy dependent cross sections for all three products enables the evaluation of experimental BDEs, which are compared to theoretical values. Theory is also used to evaluate potential energy profiles for all possible reactions. Combined with prior work on $PtO^+$ and $PtO_2^+$,[21, 23] the present results allow determination of the first and second oxide and sulfide BDEs to $Pt^+$. In addition, by combining the present thermochemistry for $PtS^+$ with a literature value for $D_0(PtS)$,[24] an improved ionization energy for PtS is derived.

## EXPERIMENTAL AND COMPUTATIONAL SECTION

### Experimental details

This work was performed using a GIBMS that has been described in detail previously.[25] Briefly, the ion source was a direct current discharge and flow tube (DC/FT),[26] in which argon was ionized by a strong electric field (1.2 – 1.5 kV) that sputtered a platinum foil sample held by the cathode to form the $Pt^+$ reactant ions. The ions were swept by the carrier gas (90%:10% He:Ar at ~0.4 Torr) along the flow tube, where the ions underwent approximately $10^5$ thermalizing collisions. The electronic states of atomic metal cations generated in this source can generally be characterized by an effective temperature of 700 ± 400 K.[27-32] In this temperature range, 99.7 – 100% pure ground level $Pt^+$ ($^2D_{5/2}$) ions were created, such that the average electronic energy, $E_{el}$, is <2 meV.[19, 33, 34] In previous studies of $Pt^+$ reacting with $O_2$ and $CO_2$,[21] there was evidence of small amounts (0.03 – 0.06%) of excited electronic states with excitation energies above 3.1 eV. These prior results are consistent with observations made here (see below). In the present work, the magnitude of the total exothermic cross section observed when compared to the collision cross section estimated using the trajectory method of Su and Chesnavich[35] indicates that the population of these excited states is only ~0.08 ± 0.01% (presuming they react with unit efficiency). In our

previous work,[21] quenching gases (either $O_2$ or $N_2O$) were introduced into the flow tube to remove the excited states. Importantly, the endothermic parts of the cross sections observed in these studies were the same before and after admission of the quenching gas, hence addition of quenching gases was not employed in the current work. Overall, these results indicate that the presence of the excited states can be attributed to a very small percent of metastable ions that are not effectively quenched by interactions with Ar and He and that the remaining ions (>99.9%) can be characterized by the 700 ± 400 K temperature.

Atomic platinum ions were extracted from the flow tube, mass analyzed for $^{195}Pt^+$ (33.8 % natural abundance) with a magnetic sector momentum analyzer, decelerated to a specific kinetic energy, and focused into an octopole ion beam guide that constrained the ions radially using radio frequency (rf) electric fields.[36, 37] A reaction cell (effective length = 8.26 cm) surrounds a section of the octopole and was filled with 0.1 – 0.4 mTorr of the $SO_2$ reactant neutral. These pressures are sufficiently low to minimize multiple collisions, although one product exhibits a pressure dependent cross section (as detailed below). Single collision cross sections for this product were obtained by extrapolating the data to zero $SO_2$ pressure. Ions were extracted from the octopole, mass analyzed in a quadrupole mass filter, and detected with a scintillation detector.[38] Utilizing procedures established previously, the absolute reaction cross sections were calculated by combining the product and total ion intensities after corrections for background signals obtained with no $SO_2$ in the collision cell.[39] Absolute cross sections have uncertainties of ±20% with ±5% relative uncertainties. Laboratory (lab) frame energies were converted to center-of-mass (CM) frame energies using $E_{CM} = E_{lab} \times m/(m + M)$, where $m$ and $M$ are the masses of the neutral and ionic reactants, respectively. As described previously, the cross sections are broadened by the thermal motion of the reactant neutral and the kinetic energy distribution of the reactant ions.[40, 41] A retarding analysis in the octopole ion guide was used to determine the full width at half maximum (fwhm, here about 0.15 eV, CM) and the absolute zero of the kinetic energy of the reactant ions.[39] The uncertainty in the absolute energy scale is ±0.012 eV (CM).

**Data analysis**

Endothermic reaction cross sections were modeled with the modified line-of-centers (MLOC) model, Eq. (1).

$$\sigma(E) = \sigma_0 \Sigma g_i (E + E_{el} + E_i - E_0)^n/E \quad (1)$$

Hhere, $\sigma_0$ is an energy-independent scaling parameter, $E$ is the center-of-mass frame kinetic energy, $E_{el}$ is the average electronic energy of $Pt^+$ (noted above), $E_i$ is the internal energy of the neutral reactant with rovibrational states $i$ having populations of $g_i$ ($\Sigma g_i = 1$) at the reaction cell temperature of 305 K, $E_0$ is the threshold energy at 0 K, and $n$ is an empirical fitting parameter. The MLOC model was convolved with the kinetic energy distributions of both neutral and ionic reactants before comparing to the experimental data.[39, 41] The parameters, $\sigma_0$, $E_0$, and $n$ were optimized using a nonlinear least-squares algorithm in order to reproduce the experimental reaction cross sections. The modeling parameters have uncertainties that were assessed by analyzing multiple data sets over a range of acceptable $n$ values. The uncertainty for $E_0$ includes the absolute uncertainties in $E_{el}$ and the CM energy scale.

When collision energies exceed the neutral bond energies of $D_0$(OS-O) and $D_0$(S-$O_2$), dissociation of the product ions can ensue. This behavior can be reproduced by modifying Eq. (1) with the dissociation probability, $P_D$, previously described.[42] Two parameters control $P_D$: $p$, similar to $n$ but limited to integral values, and $E_D$, the energy where the product ion can begin to dissociate. In our analysis, $p$ and $E_D$ were optimized in order to accurately model the experimental data but without affecting determinations of $E_0$.

The $E_0$ threshold energies resulting from the modified line-of-centers modeling were converted to product ion BDEs using Eqs. (2) and (3),

$$D_0(Pt^+\text{-L}) = D_0(\text{OS-O}) - E_0 \quad (\text{L} = \text{O or SO}) \quad (2)$$

$$D_0(Pt^+\text{-L}) = D_0(\text{S-O}_2) - E_0 \quad (\text{L} = \text{S or O}_2) \quad (3)$$

where $D_0$(OS-O) = 5.661 ± 0.014 eV and $D_0$(S-$O_2$) = 5.900 ± 0.003 eV.[43] Eqs. (2) and (3) implicitly assume that no activation barrier in excess of the endothermicity is present in the associated reaction. The long-range attractive force between ions and molecules generally means that this

assumption is valid.[39, 44] Further, the theoretical potential energy profiles are consistent with this hypothesis with one possible exception discussed below.

**Theoretical calculations**

Quantum chemistry calculations were conducted using the Gaussian16 suite of programs.[45] In our previous work on reactions of $Re^+$, $Os^+$, and $Ir^+$ with small molecules, thermochemistry in agreement with experiment[14-19, 33, 34, 52, 53] was found using B3LYP hybrid density functional theory[46, 47] and coupled cluster with single, double, and perturbative triple excitations, CCSD(T),[48-51] levels of theory. Here, we calculated optimized geometries and vibrational frequencies (used unscaled) at both the B3LYP and CCSD(T) levels of theory, although for a couple of species, single point calculations at the CCSD(T) level were performed using optimized structures obtained at the B3LYP level because the CCSD(T) geometry optimizations failed. For product ions, various electronic states were explored by varying the orbital occupation before geometry optimization. States were assigned on the basis of the symmetry of the orbitals occupied. Def2-XZVPPD (X = T and Q) and aug-cc-pVXZ (X = T, Q, and 5)[54-56] basis sets imported from the EMSL basis set exchange[57, 58] were utilized in the present work. For $Pt^+$, these basis sets use an effective core potential (ECP) having a small core (60 electrons) with explicit 5s, 5p, 5d, and 6s valence orbitals. Additionally, we performed complete basis set (CBS) extrapolations using two point (Q, 5) protocols according to the Karton-Martin method,[59] Eq. (4), for Hartree-Fock (HF) energies (where Y = 4 or 5).

$$E_Y = E_{CBS} + A(Y + 1)e^{-6.57\sqrt{Y}} \quad (4)$$

The CBS limit for the correlation energy was calculated using the same basis sets and Eq. (5).[60]

$$E_Y = E_{CBS} + B(Y + ½)^{-4} \quad (5)$$

As these approaches utilize single-reference based wave functions, the multireference character of the reactants and product ions was checked using the T1 diagnostic,[61] where values exceeding 0.045 are judged to be "somewhat less reliable" for open shell species.[62] We find that $Pt^+$ ($^2$D) has a value of 0.013 and $PtS^+$ ($^4\Sigma$) has 0.044, suggesting that the single reference approach should be adequate. For $PtO^+$ ($^4\Sigma$) and $PtSO^+$ ($^2$A'), the values are 0.060 and 0.053, indicating that

calculations including multireference character may be desirable, but are beyond the scope of the present study.

Calculated BDEs of $SO_2$ are in reasonable agreement (within ~10% deviation) with experiment[43] at all levels of theory, as detailed in previous work.[14, 15] For example, the B3LYP/def2-TZVP level of theory used to examine the potential energy profiles yields 5.25, 5.39, and 5.37 eV for the OS-O, S-$O_2$, and SO BDEs, compared to experimental values of 5.661 ± 0.014, 5.900 ± 0.003, and 5.356 ± 0.014 eV, respectively.[43] However, because these theoretical OS-O and S-$O_2$ BDEs are weak by 0.4 – 0.5 eV, this does lead to discrepancies in the overall reaction endothermicities calculated at this level, see below. Results from the CCSD(T) level generally show < 1% deviation, e.g., CCSD(T)/CBS//CCSD(T)/aug-cc-pVTZ values are 5.66, 5.92, and 5.33 eV, respectively. Vibrational frequencies of $SO_2$ also agree well with experimental values[43] at almost all levels used.[14, 15]

## EXPERIMENTAL RESULTS

### Reactions of $Pt^+$ with $SO_2$

The kinetic energy dependent product ion cross sections obtained from reactions of $Pt^+$ with $SO_2$ are shown in Figure 1. A simple association of $Pt^+$ and $SO_2$ is suggested by observing that $PtSO_2^+$ is formed in a barrierless exothermic reaction at the lowest energies. This product cross section is found to depend linearly on $SO_2$ pressure, such that this cross section disappears upon extrapolation to zero-pressure (rigorous single collision conditions), indicating that $PtSO_2^+$ is formed by collisional stabilization. At the same low energies, the other three products, $PtO^+$, $PtSO^+$, and $PtO_2^+$/$PtS^+$ also exhibit small cross sections that rapidly decrease with increasing energy and are also pressure dependent. These exothermic pathways therefore appear to be associated with a contribution from an excited electronic state of $Pt^+$ or perhaps multiple collision events. As noted above, this observation is consistent with previous studies.[21] The magnitude of these exothermic cross sections indicates the excited state population is <0.1%.

At higher energies, the cross sections are no longer dependent on $SO_2$ pressure. Here, the

products observed correspond to reactions (6) – (9), which all exhibit thresholds.

$$Pt^+ (^2D_{5/2}) + SO_2 (^1A_1) \rightarrow PtO^+ + SO \quad (6)$$

$$\rightarrow PtSO^+ + O \quad (7)$$

$$\rightarrow PtO_2^+ + S \quad (8a)$$

$$\rightarrow PtS^+ + O_2 \quad (8b)$$

$$\rightarrow PtS^+ + 2\,O \quad (9)$$

Reaction (6) has the lowest energy threshold. The cross section for $PtO^+$ rises quickly, reaching a plateau near 4 eV before decreasing slowly at energies above the BDE of the neutral reactant, $D_0$(OS-O) = 5.66 eV, which can be attributed to dissociation of the product ion into $Pt^+ + O$. Previous GIBMS studies of the reactions of $Pt^+$ with $O_2$, CO, $CO_2$, and NO provided measurements of $D_0(Pt^+\text{-O})$ of 3.26 ± 0.05, 3.27 ± 0.05, 3.26 ± 0.08, and 3.26 ± 0.10 eV, for a weighted average of 3.26 ± 0.07 eV (two standard deviations of the mean), as listed in Table I.[21, 63] This agrees with an upper limit of ≤ 3.164 eV from photodissociation measurements by Metz and co-workers.[64] Notably, in subsequent work,[65] Metz and co-workers adopted the value of 3.26 ± 0.07 eV for their calculation of the BDE for PtO, and we will do likewise here for the remainder of the paper. Using Eq. (2), this BDE suggests that the threshold for reaction (6) should occur at 2.40 ± 0.07 eV, in qualitative agreement with the apparent threshold near 2 eV.

At slightly higher energies, the $PtSO^+$ cross section starts and reaches a maximum near $D_0$(OS-O). The sum of the $PtO^+$ and $PtSO^+$ cross sections changes smoothly with energy and reaches a maximum in good agreement with $D_0$(O-SO). This behavior suggests that these two products compete with one another. The $PtSO^+$ cross section declines more rapidly above $D_0$(O-SO) than the $PtO^+$ cross section because the atomic oxygen neutral product of reaction (7) can carry away less energy than the heavier diatomic SO neutral product of reaction (6). The ionic products of reactions (8) and (9) cannot be distinguished in this instrument as they have the same nominal mass. This cross section exhibits two clear features: a very small cross section just above the noise level (more apparent at higher $SO_2$ pressures) that begins near 4 eV and peaks near 6 eV, and a larger feature starting near 7 eV. As discussed further below, this second feature is assigned to

reaction (9), otherwise the observed threshold energy cannot be interpreted meaningfully. Previous studies determined $D_0(OPt^+\text{-}O) = 3.06 \pm 0.07$ eV and $D_0(Pt^+\text{-}O_2) = 1.20 \pm 0.10$ eV from GIBMS measurements of reactions of $PtO^+$ with $O_2$ and $CO_2$ and CID of $PtO_2^+$ formed by reactions of $Pt^+$ with $N_2O$.[23] This thermochemistry indicates that the threshold for reaction (8a) should be 4.70 ± 0.07 eV, well above the apparent threshold. This observation suggests that reaction (8b) is responsible for the lower energy feature, a conclusion that can be checked by the thermochemistry derived below.

**MLOC modeling of reaction cross sections**

The MLOC model of Eq. (1) was used to reproduce the cross sections in the threshold regions, as shown in Fig. 2. Modeling parameters of Eq. (1) for all channels are included in Table II. For the $PtO^+$ channel, complications associated with competition with the $PtSO^+$ product were avoided by modeling the total cross section. Fig. 2 shows that this model accurately reproduces the total cross section over three orders of magnitude and from threshold to ~10 eV. The threshold of $E_0 = 2.52 \pm 0.11$ eV is in good agreement with the threshold predicted using the literature thermochemistry: 2.40 ± 0.07 eV. The MLOC model also allows accurate reproduction of the $PtSO^+$ cross section over a similar extended range of energies and magnitudes, Fig. 2.

The cross section for the $PtO_2^+/PtS^+$ channel exhibits two features corresponding to reactions (8) and (9). The lower energy feature is sufficiently noisy that an unambiguous analysis is not possible; therefore, its interpretation is performed in a self-consistent manner with the higher energy feature presuming that reactions (8b) and (9) are responsible for the two features. As noted above, this conclusion is consistent with the apparent threshold observed lying below that predicted for formation of $PtO_2^+$ in reaction (8a). Therefore, we first modeled the low-energy cross section feature using the MLOC model, including the $P_D$ model for further dissociation of the product, Fig. 2, and then subtracted this model from the experimental data. The residual high-energy cross section was independently analyzed with the resulting parameters in Table II. Because this threshold lies above $D_0(S\text{-}O_2)$, it can only be interpreted from a thermodynamic point of view if this feature corresponds to reaction (9). Further, if the lower energy feature corresponds

to reaction (8b), then its threshold should lie $D_0(O_2)$ = 5.117 eV below that for reaction (9) (presuming no extra barrier for reaction). The MLOC models shown in Fig. 2 use thresholds for reactions (8b) and (9) that are self-consistent in this fashion, as shown in Table II. The combination of these two models reproduces the observed cross section with fidelity over the entire experimental energy range.

In our previous studies of the reactions of $Re^+$, $Os^+$, and $Ir^+$ with $SO_2$, we also utilized a phase space theory (PST) approach[66-68] to model the data as this accounts for competition between the various channels. In all three systems, the MLOC modeling yielded threshold energies that agreed better with existing thermodynamic data. Attempts to use the PST model in the present system yielded similar results and also suggested that the $PtSO^+$ channel could be composed of several pathways. As the PST model does not improve our thermodynamic analysis here, we have chosen not to pursue this approach further.

**$PtO^+$ thermochemistry**

Available literature thermochemistry for the $PtO^+$ species has been discussed in previous work.[21] As noted above, previous GIBMS studies of the reactions of $Pt^+$ with $O_2$, CO, $CO_2$, and NO provided a value for $D_0(Pt^+\text{-}O)$ of 3.26 ± 0.07 eV,[21, 63] and the photodissociation limit is ≤ 3.164 eV,[64] Table I. For reaction (6), by using Eq. (2) and the MLOC threshold listed in Table II (2.52 ± 0.11 eV), the BDE of $Pt^+$-O is obtained as $D_0(Pt^+\text{-}O)$ = 3.14 ± 0.11 eV. This value agrees very well with the previous GIBMS values and the photodissociation result, Table I. If we were to combine the present BDE with the previous four GIBMS values, the weighted average would change slightly to 3.25 ± 0.06 eV (two standard deviations of the mean).

**$PtO_2^+$/$PtS^+$ thermochemistry**

Cross sections for the $PtO_2^+$/$PtS^+$ products show two obvious features, Figs. 1 and 2. The $PtO_2^+$/$PtS^+$ cross sections are well reproduced over the entire energy experimental range with two contributions as shown in Fig. 2. As noted above, the thresholds for the two features were determined in a self-consistent fashion to differ by $D_0(O_2)$ such that using the measured thresholds in Eq. (3) leads to $D_0(Pt^+\text{-}O_2)$ or $D_0(Pt^+\text{-}S)$ = 3.68 ± 0.31 eV. Previous GIBMS work established

that $D_0(Pt^+-O_2)$ = 0.67 ± 0.05 for a $Pt^+(O_2)$ adduct or 1.20 ± 0.10 eV for the inserted $OPtO^+$ structure.[23] Thus, the value obtained here must correspond to formation of $PtS^+$ at both low and high energies. The observation that the $PtS^+$ BDE (3.68 ± 0.31 eV) is similar to that for the isovalent $PtO^+$ (3.26 ± 0.07 eV) is also consistent with this assignment. Although no literature values are available for $D_0(PtS^+)$, this conclusion can be further evaluated by comparison with theoretical calculations.

Recently, the 0 K BDE for neutral PtS has been measured using predissociation spectroscopy by Morse and co-workers as 4.144 ± 0.008 eV.[24] This value can be combined with the present $PtS^+$ BDE in the relationship $D_0(PtS) + IE(Pt) = D_0(PtS^+) + IE(PtS)$ to yield a value for IE(PtS) given IE(Pt) = 72257.8 ± 0.8 $cm^{-1}$ = 8.9588 ± 0.0001 eV.[69] This procedure yields IE(PtS) = 9.42 ± 0.31 eV. As for PtO, where IE(PtO) has been determined by photoionization as 10.0 ± 0.1 eV,[65] the IE is greater than that for atomic Pt, or equivalently, the BDEs of the diatomic platinum chalcogenides cations are weaker than those of the corresponding neutrals.

**$PtSO^+$ thermochemistry**

In Fig. 2, the endothermic cross section of the $PtSO^+$ product was modeled using the MLOC model, Eq. (1). The threshold value of 2.63 ± 0.12 eV is used in Eq. (2) to obtain $D_0(Pt^+-SO)$ of 3.03 ± 0.12 eV, Table I. Note that this value does not imply anything about the structure of the $PtSO^+$ product. Combining this value with $D_0(SO)$ = 5.356 ± 0.014 eV[43] and $D_0(PtO^+)$ = 3.26 ± 0.07 eV indicates that $D_0(OPt^+-S)$ = 5.13 ± 0.14 eV. Using $D_0(PtS^+)$ = 3.68 ± 0.31 eV, one obtains $D_0(SPt^+-O)$ = 4.71 ± 0.31 eV. There are no literature values available for the $Pt^+$-SO BDE, such that theoretical calculations were performed for $D_0(Pt^+-SO)$ for comparison, as detailed below. Note that $D_0(OPt^+-S)$ and $D_0(SPt^+-O)$ lie 1.45 eV above $D_0(Pt^+-S)$ and $D_0(Pt^+-O)$, respectively, and are more similar to $D_0(SO)$ = 5.356 eV.

## THEORETICAL RESULTS

Previous work has included extensive calculations at several levels of theory for $PtO^+$ and $PtO_2^+$.[21, 23, 70, 71] The most pertinent results are compared to the experimental data in Table I . In

the present work, possible states of $PtS^+$, $PtSO^+$, and $PtSO_2^+$ was surveyed at the B3LYP/def2-TZVPPD level and then higher levels of theory were applied to the lowest energy electronic states located for $PtO^+$, $PtO_2^+$, $PtS^+$, and $PtSO^+$.

The ground states of the $PtO^+$ and $PtS^+$ products were determined after including spin-orbit (S.O.) effects. For $PtO^+$, Heinemann et al.[71] have calculated S.O. corrections of 0.20 and 0.16 eV for the $^4\Sigma_{3/2}^-$ and $^2\Sigma_{1/2}^-$ states. Here, we estimate that the $^2\Pi_{1/2}$ and $^4\Delta_{7/2}$ excited states have S.O. corrections of 0.26 eV = $\zeta_{5d}(Pt)/2$ and 0.52 eV = $\zeta_{5d}(Pt)$ (where = $\zeta_{5d}(Pt)$ = 4221 $cm^{-1}$)[72] using a semi-empirical approach.[17-19, 34, 72, 73] We presume that the same values hold for the analogous $PtS^+$ states. The $PtSO^+$, $PtO_2^+$, and $PtSO_2^+$ species have no first order S.O. corrections because their orbital angular momentum is zero. BDE values also require a S.O. correction to the asymptotic products because the calculations produce values at the weighted average of S.O. levels. Here, we use experimental values for the ground J levels of O, S, and $Pt^+$, which lie 0.0097, 0.024, and 0.418 eV, respectively, lower than the average of the weighted J levels.[69]

In the discussion below, only valence electrons are included in the molecular orbital (MO) configurations, without specifying the 1s and 2s core electrons on O, 1s, 2s, 2p, and 3s core electrons on S, and the 1s–5s, 2p–5p, and 3d–4d core electrons of platinum. For the diatomic $PtL^+$ species, the bonding MOs are 1σ and 1π, non-bonding MOs are 1δ and 2σ (mostly 6s on platinum), and anti-bonding MOs are 2π and 3σ.

**$PtO^+$**

Previous work has identified the ground state (GS) of $PtO^+$ as $^4\Sigma^-$ with a $1\sigma^2 1\pi^4 1\delta^4 2\sigma^1 2\pi^2$ electron configuration.[21, 71] Low-lying excited states include $^2\Sigma^-$ ($1\sigma^2 1\pi^4 1\delta^4 2\sigma^1 2\pi^2$), $^2\Pi$ ($1\sigma^2 1\pi^4 1\delta^4 2\pi^3$), and $^4\Delta$ ($1\sigma^2 1\pi^4 1\delta^3 2\sigma^2 2\pi^2$). A manifold of higher lying states have also been identified (with excitation energies of 0.92 – 1.80 eV).[71] To verify what level of theory is adequate for the other species examined in the present work, we performed additional calculations for the three lowest lying states of $PtO^+$. The results shown in Table III uniformly obtain $^4\Sigma^-$ as the GS, with the $^2\Sigma^-$ lying 0.54 – 0.62 eV higher in energy, the $^4\Delta$ lying 0.66 – 0.71 eV above the GS, and the $^2\Pi$ state lying 0.89 – 1.18 eV higher. These excitation energies are in reasonable agreement

with vertical excitation energies (at 1.80 Å) obtained by Heinemann, Koch, and Schwarz of 0.51, 1.08, and 0.83 eV, respectively.[71] Our relative energies include the S.O. corrections noted above, such that the true GS is $^4\Sigma_{3/2}^-$. Bond lengths calculated here for the GS range from 1.730 – 1.737 Å with vibrational frequencies being 813 – 831 $cm^{-1}$. These values are comparable with results from with previous calculations of 1.805 Å and 675 $cm^{-1}$ (CAS-SCF/TZPP[71]) and 1.736 Å and 799 $cm^{-1}$ (MR-QDPT[70]).

The BDE value for the $^4\Sigma_{3/2}^-$ GS of $PtO^+$ calculated at the B3LYP/def2-TZVPPD level and including the S.O. correction of 0.228 (= 0.418 + 0.0097 – 0.20) eV is 3.14 eV. Other values in Table III range from 2.92 to 3.24 eV with the CCSD(T)/CBS//CCSD(T)/aug-cc-pVTZ value being 3.10 eV. These theoretical values agree well with the GIBMS and photodissociation experimental values, as well as with literature theoretical values, Table I.

**$PtS^+$**

Because $PtS^+$ is isovalent with $PtO^+$, we only calculated the four lowest energy states: $^4\Sigma^-$, $^2\Sigma^-$, $^2\Pi$, and $^4\Delta$. As shown in Table IV, the GS remains $^4\Sigma^-$ with the $^2\Pi$, $^4\Delta$, and $^2\Sigma^-$ states lying 0.05 – 0.36, 0.11 – 0.18, and 0.37 – 0.45 eV higher in energy, respectively. As noted above, S.O. corrections for these three states were presumed to match those of $PtO^+$, leading to a GS of $^4\Sigma_{3/2}^-$. The bond length of $PtS^+$ is longer than that for $PtO^+$ by 0.34 – 0.36 Å, consistent with the difference in covalent radii of O and S: 0.74 and 1.04 Å, respectively.[74] Likewise, the vibrational frequency drops from 813 – 831 $cm^{-1}$ to 469 – 495 $cm^{-1}$ because of the heavier ligand. The theoretical BDE for $PtS^+$ ($^4\Sigma_{3/2}^-$) (after S.O. corrections of -0.24 eV) ranges from 3.44 – 3.74 eV with the CCSD(T)/CBS//CCSD(T)/aug-cc-pVTZ value being 3.70 eV. These predictions are in good agreement with the experimental value of 3.68 ± 0.31 eV. This comparison bolsters the conclusion reached above that the cross section observed experimentally can be assigned to $PtS^+$ rather than $PtO_2^+$.

**$PtO_2^+$**

In previous work, possible states of $PtO_2^+$ were investigated at several levels of theory including density functional theory (DFT: B3LYP and BP86) approaches and higher order multi-

reference perturbation theory (MR-PT) approaches, either (MC-QDPT) or complete active space (CASPT2) levels.[70] The DFT approaches generally predict that a $PtOO^+$ ($^2A$) structure is favored (both in this work and by Zhang and Armentrout[23]), whereas the PT approaches clearly find a linear $OPtO^+$ ($^2\Sigma_g^+$) ground state. The latter result agrees with GIBMS experiments, which place the $PtOO^+$ structure 0.53 ± 0.11 eV above the inserted $OPtO^+$ species.

Here, we double check the GS assignment by performing high-level calculations for the lowest energy states found previously. As commented on before,[70] calculation of the $PtOO^+$ structure is problematic and would not easily converge for CCSD(T) calculations in general. As before,[70] B3LYP geometry optimizations of the $OPtO^+$ structure led to a bent geometry when using the def2-TZVPPD basis set, but CCSD(T) and B3LYP/aug-cc-pVTZ calculations converge to a linear structure. As shown in Table V, for all but the B3LYP/def2-TZVPPD level, the GS remains $^2\Sigma_g^+$ with excitation energies for $PtOO^+$ ($^2A''$) structures ranging from 0.80 – 0.92 eV for the CCSD(T) calculations. The $PtOO^+$ ($^2A''$) had unsymmetric Pt-O bond lengths at the B3LYP levels of theory, but the CCSD(T)/aug-cc-pVTZ calculation yielded a $^2A_2$ state having $C_{2v}$ symmetry. This species can be viewed as a $Pt^+(O_2)$ adduct. We also looked for a $^2A'$ state of $PtOO^+$, but this generally collapsed to the linear $OPtO^+$ structure.

The $^2\Sigma_g^+$ GS of $OPtO^+$ is found to have a BDE for loss of one oxygen ligand of 3.22 – 3.47 eV after the S.O. corrections at the CCSD(T) levels of theory (B3LYP gives lower values, Table V), with the highest value being CCSD(T)/CBS//CCSD(T)/aug-cc-pVTZ. Alternatively, the BDEs for loss of molecular $O_2$ from $OPtO^+$ are 1.31 – 1.56 eV (with B3LYP values again being lower). These results are slightly higher than the experimental values of 3.06 ± 0.07 and 1.20 ± 0.10 eV, respectively.[23] For the present purposes, the latter value is much less than the BDE that would be obtained from analysis of the $PtS^+/PtO_2^+$ cross section, 3.68 ± 0.31 eV. Thus, the conclusion that this cross section is associated with $PtS^+$ formation seems unambiguous.

**$PtSO^+$**

Various geometries and low-lying excited states of $PtSO^+$ calculated at the B3LYP/def2-TZVPPD level are listed in Table VI. This is undoubtedly not an exhaustive compilation of all

possible states. The lowest energy structure was a $PtSO^+$ ($^2A'$) adduct having doublet spin in which the SO ligand binds to platinum via the sulfur atom. The lowest-lying excited state is $Pt^+(OS)$ ($^2A''$), in which the oxygen is also bound to platinum, forming a side-on adduct. A $PtSO^+$ ($^4A'$) state, with a structure similar to the ground state, lies 1.10 eV higher in energy. Finally, inserted structures, $OPtS^+$, having ∠SPtO bond angles of 110 - 127° were located with doublet and quartet spins. These inserted structures lie ~1.9 eV above the GS.

To verify the true GS of $PtSO^+$, the two lowest energy states in Table VI along with the lowest energy inserted structure were also calculated at higher levels of theory, Table VII. All calculations indicate the $^2A'$ state remains the GS with the $Pt^+(OS)$ species remaining about 0.5 eV above the GS. The inserted $OPtS^+$ ($^2A'$) structure lies much higher in energy, 1.57 – 2.02 eV above the $^2A'$ GS. The $PtSO^+$ ($^2A'$) GS is calculated to have a $Pt^+$-SO BDE of 2.63 – 2.96 eV after S.O. corrections for the $Pt^+$ asymptote are applied, with the highest value corresponding to the CCSD(T)/CBS result. This BDE, in particular, is in good agreement with the experimental value of 3.03 ± 0.12 eV, Table I.

**Potential energy profiles of $PtSO_2^+$**

The potential energy profiles of the $PtSO_2^+$ system were also studied at the B3LYP/def2-TZVPPD level and are shown in Fig. 3 with corresponding structures for doublet spin states in Fig. 4. The geometrical parameters of these structures are listed in Table SI in the supplementary material. All energies are relative to GS reactants, $Pt^+$ ($^2D_{5/2}$) + $SO_2$ ($^1A_1$), after S.O. corrections of 0.418 eV for the $Pt^+$ ($^2D_{5/2}$) reactant, 0.584 eV for the $Pt^+$ ($^4F_{9/2}$) reactant,[69] 0.20 eV for the $^4\Sigma_{3/2}^-$ states of both $PtO^+$ and $PtS^+$ products,[71] and 0.010 eV for the O product.

**Doublet spin surfaces**

GS reactants couple to form a planar $SO_2$ adduct, **$^2$1** $Pt^+(OSO)$ ($^2A'$), lying 1.30 eV lower in energy. As only one O atom is bound to the Pt atom, the $SO_2$ ligand is nearly unperturbed with vibrational frequencies (545, 1046, 1347 $cm^{-1}$, Table SI) similar to those in molecular $SO_2$ (519, 1178, 1377 $cm^{-1}$).[14] The **$^2$1** intermediate can rearrange to a different adduct by swinging the outermost oxygen further away from Pt. This path passes over **$^2$TS1/1'** (imaginary frequency of

108i $cm^{-1}$) at 1.08 eV below reactants to form $^2$**1'** ($^2$A'), 1.11 eV below reactants. A comparable adduct having A" symmetry ($^2$**1"**) was located another 0.19 eV higher in energy. The $^2$**1'** intermediate can activate an SO bond to form $^2$**2** ($OPt^+SO$, $^2$A) by passing over $^2$**TS1'/2**. In this TS, the S-O bond nearest Pt breaks as the sulfur migrates towards Pt to form a Pt-S bond (imaginary frequency of 200i $cm^{-1}$). Both $^2$**TS1'/2** and $^2$**2** are nonplanar and lie 0.66 and 0.28 eV above GS reactants, respectively. Rotation about the Pt-S bond of $^2$**2** passes through two planar transition states ($^2$**TS2/cis** and $^2$**TS2/trans**) (Table SI and Fig. S1) having A" symmetry, 0.17 eV above $^2$**2** when the oxygens are cis to one another and 0.07 eV higher when they are trans. The $^2$**2** intermediate can also rearrange to a more stable intermediate, $^2$**2'** (only 0.10 eV above GS reactants) by bringing the distant O atom closer to Pt over $^2$**TS2/2'** (241i $cm^{-1}$), which lies 0.13 eV higher in energy than $^2$**2**.

$PtO^+$ ($^4\Sigma_{3/2}^-$) + SO ($^3\Sigma^-$) products, calculated to lie 2.12 eV (2.40 ± 0.07 eV experimental, 2.56 eV CCSD(T)/CBS) above GS reactants, can be formed from $^2$**2** or $^2$**2'** by cleaving the Pt-SO bond (which is spin-allowed because the products can couple to form intermediates along doublet, quartet, and sextet spin surfaces). The deviation from experiment for the B3LYP/def2-TZVPPD energy lies chiefly in its underestimate of the O-SO BDE, as noted above. Alternatively, cleavage of the PtO bond in $^2$**2** or $^2$**2'** can directly form $PtSO^+$ ($^2$A') + O ($^3$P), calculated to lie 2.62 eV (2.63 ± 0.12 eV experimental, 2.70 eV CCSD(T)/CBS) above GS reactants. (Here, the B3LYP/def2-TZVPPD level underestimates both the OS-O and $Pt^+$-SO BDEs.) Neither of these spin-allowed dissociations have a barrier lying higher in energy than the products, Fig. 3.

Alternatively, $^2$**2** can pass over $^2$**TS2/3** (1.71 eV above reactants) to form the planar, cyclic $cPt^+SOO$, $^2$**3** ($^2$A') at 1.40 eV above reactants. In this process, the two oxygens approach one another to form a bond, with an imaginary frequency of 520i $cm^{-1}$. Cleavage of the Pt-O bond over $^2$**TS3/4** (2.08 eV above GS reactants) leads to $^2$**4**, $SPt^+(O_2)$ ($^2$A'), in which a dioxygen molecule attaches to the Pt in $PtS^+$ ($^4\Sigma^-$). This intermediate is presumed to have the same S.O. correction as the $PtS^+$ ($^4\Sigma^-$) product, 0.20 eV, because the $O_2$ is weakly bound to the $PtS^+$ cation. Loss of the $O_2$ adduct requires only 0.11 eV and leads to formation of $PtS^+$ ($^4\Sigma^-$) + $O_2$ ($^3\Sigma_g^-$) in a spin-allowed

process (again because the product spin states can couple along doublet, quartet, and sextet spin surfaces). Here, the products are calculated to lie 1.71 eV (2.22 ± 0.31 eV experimental, 2.22 eV CCSD(T)/CBS) above GS reactants. We also located two additional $PtS^+(O_2)$ adducts, **$^2$4'** ($^2$A') and **$^2$4'** ($^2A_2$) (Table SI and Fig. S1) that lie 0.16 and 0.13 eV below **$^2$4**, respectively; however, these species are formed by coupling the $PtS^+$ ($^4\Delta$) and $PtS^+$ ($^2\Pi$) states with $O_2$, such that these species should not easily lead to the $PtS^+$ ($^4\Sigma^-$) ground state product. Here, the two oxygen atoms bind to Pt with fairly short bonds (1.99 – 2.22 Å, Fig. S1), in contrast to the **$^2$4** intermediate, where $O_2$ binds to S and is remote from Pt, Fig. 4.

One interesting aspect of the reaction of $Pt^+$ with $SO_2$ is that theory and experiment agree that formation of $PtS^+$ + SO is the lowest energy process among the three product channels observed, yet this product channel is the least efficient, Fig. 1. The reaction coordinate diagram of Figure 3 helps explain this observation because the intermediates leading to $PtO^+$ + SO and $PtSO^+$ + O (**$^2$2** and **$^2$2'**) occur early along the potential energy surface and readily dissociate to these products through loose transition states. In contrast, elimination of $O_2$ to yield $PtS^+$ requires passing over the two high-energy TSs, **$^2$TS2/3** and **$^2$TS3/4**, making this pathway entropically much less favorable. As a consequence, even though the modeling shown in Fig. 2 has $PtS^+ + O_2$ with a threshold lower than those for formation of $PtO^+$ + SO and $PtSO^+$ + O (2.2 eV versus 2.5 and 2.6 eV, Table II), the $PtS^+$ cross section is much smaller. Theory at the B3LYP/def2-TZVPPD level also suggests that **$^2$TS3/4** is higher in energy than the $PtS^+ + O_2$ product asymptote (by 0.16 eV before S.O. corrections and 0.36 eV after the 0.20 S.O. correction for $PtS^+$). To check this result, single point calculations at the CCSD(T)/def2-XZVPPD//B3LYP/def2-TZVPPD (X = T and Q) were performed and lead to **$^2$TS3/4** lying 0.36 – 0.39 eV (increasing by 0.20 if the S.O. correction is applied) above $PtS^+ + O_2$ products. Notably, if these energies are used in the modeling of the low-energy feature of the $PtS^+$ cross section, the data can still be reproduced well within the considerable scatter of this cross section feature.

**Quartet spin surfaces**

Some calculations for quartet spin intermediates were also conducted. The quartet surfaces

start from excited state reactants, $Pt^+$ ($^4F_{9/2}$) + $SO_2$ ($^1A_1$), calculated to lie 0.61 eV above the $^2D_{5/2}$ GS reactant after S.O. corrections (compared to 0.593 eV experimentally).[69] The $Pt^+(OSO)$ ($^4A_1$) adduct (Fig. S1) binds both oxygens symmetrically to $Pt^+$ but lies 1.64 eV higher in energy than $^2$**1** because the occupied 6s electron on $Pt^+$ ($^4F$) yields a repulsive interaction with the closed shell $SO_2$ ligand. Likewise, the quartet spin analogue of the $^2$**2** $OPt^+SO$ inserted product lies 0.33 eV higher in energy. In contrast, the analogue of $^2$**2'** $OPt^+(SO)$ lies 0.04 eV lower in energy. Therefore, it is possible that there is coupling between the doublet and quartet surfaces in the region of the $^2$**2** and $^2$**2'** intermediates, but this seems unlikely to influence the progress of the reaction compared with remaining on the doublet surface. No analogue for the cyclic $^2$**3** $cPt^+SOO$ intermediate having quartet spin could be located, as this would collapse to another nearby structure. Finally, a quartet analogue of the $^2$**4'** $SPt^+(O_2)$ intermediate was found to lie at comparable energy. Again some coupling between the doublet and quartet spin surfaces could occur in this region, but such coupling is unlikely to change the course of the reaction appreciably. In any event, the quartet intermediates do not change the overall energetics of the processes observed.

## DISCUSSION

### Metal oxide and metal sulfide BDEs in comparison

$PtO^+$ and $PtS^+$ are isovalent. Both have $^4\Sigma^-$ GSs with equivalent valence electron configurations of $1\sigma^2 1\pi^4 1\delta^4 2\sigma^1 2\pi^2$, i.e., formation of a triple bond ($1\sigma^2 1\pi^4$), four electrons in the non-bonding 1δ, Pt(5d), along with single occupation of two antibonding 2π orbitals and 2σ, largely Pt(6s), molecular orbitals (MOs). Experimentally, the BDEs are 3.26 ± 0.07 and 3.68 ± 0.31 eV, respectively, for a difference of 0.42 ± 0.31 eV. In agreement, theory at all levels indicates that the $PtS^+$ BDE is 0.50 – 0.60 eV stronger than $PtO^+$, Tables III and IV. This is presumably a consequence of better orbital overlap between platinum and sulfur, a conjecture that is confirmed by a natural bond orbital (NBO) analysis[75, 76] at the CCSD(T)/aug-cc-pVTZ level. This shows that there is essentially no charge transfer (from metal to ligand) in $PtO^+$ (+1.03e on Pt and -0.03e on O), whereas the charge is distributed more evenly in $PtS^+$ (+0.66e on Pt and +0.34e on S). This

charge transfer occurs from the 3p orbitals of S almost entirely to Pt(6s), such that the 2σ orbital is a 6s-5d hybrid.

We can also consider the second bond energies of the platinum chalcogenide cations. The $Pt^+$-SO BDE of Table I can be combined with the reported $Pt^+$-S and $Pt^+$-O BDEs to yield $D_0(SPt^+\text{-}O) = 4.71 \pm 0.32$ eV and $D_0(OPt^+\text{-}S) = 5.13 \pm 0.14$ eV. These lie 1.45 eV above the first BDEs, $D_0(Pt^+\text{-}O) = 3.26 \pm 0.07$ eV and $D_0(Pt^+\text{-}S) = 3.68 \pm 0.31$ eV, respectively, and are more similar to $D_0(SO) = 5.356$ eV. These experimental BDEs with platinum are in reasonable agreement with values calculated at the CCSD(T)/CBS level: 4.59, 5.19, 3.10, and 3.70 eV, respectively, after S.O. corrections. These comparisons are consistent with the theoretical structure of GS $PtSO^+$ as a platinum cation with a SO ligand as opposed to an inserted $OPtS^+$ structure. This conclusion is further strengthened by noting that for the inserted $OPtO^+$ species, $D_0(OPt^+\text{-}O) = 3.06 \pm 0.07$ eV lies just below $D_0(PtO^+)$. This indicates that the formation of two covalent bonds to platinum should be more equivalent to one another, in contrast with the values obtained for $SPt^+$-O and $OPt^+$-S.

**Periodic trends in metal oxide and sulfide BDEs**

The observation that the BDE for $PtS^+$ exceeds that for $PtO^+$ is comparable to results for its lighter congener, $PdO^+$ and $PdS^+$, where the BDEs have been measured as $1.46 \pm 0.11$[77] and $2.36 \pm 0.11$ eV,[78] respectively. Carter and Goddard[79] have suggested that $PdO^+$ has a $^2\Pi$ ground state whereas our own preliminary calculations at the CCSD(T)/aug-cc-pVTZ level suggest it remains $^4\Sigma^-$ (with the $^2\Pi$ about 1.2 eV higher in energy). Likewise, these calculations indicate a $^4\Sigma^-$ ground state for $PdS^+$ with the $^2\Sigma^-$, $^4\Delta$, and $^2\Pi$ states lying about 0.3, 0.8, and 0.9 eV higher in energy. The orbital character of the $^4\Sigma^-$ states is comparable to the platinum analogues. Again, there is very ittle charge transfer on the oxide (+0.96e on Pd and +0.04e on O), whereas the sulfide involves more electron transfer but less than in the platinum analogue (+0.76e on Pt and +0.24e on S). Again the charge transfer is mainly to the Pd(5s) orbital (0.13e out of 0.24e).

In contrast, for the 3d congeners, the BDEs of $NiO^+$ and $NiS^+$ are nearly equivalent according to values measured by photodissociation: $2.535 \pm 0.025$ eV and $2.491 \pm 0.015$ eV,[80]

respectively. (GIBMS studies have determined $2.74 \pm 0.07$[81, 82] and $2.46 \pm 0.04$ eV,[83] respectively.) High-level calculations indicate the ground state of $NiO^+$ is also $^4\Sigma^-$[80, 84] whereas $NiS^+$ has nearly degenerate $^4\Sigma^-$ and $^4\Delta$ states, with spectroscopic evidence that the $^4\Delta_{7/2}$ is the true GS.[80] CCSD(T)/aug-cc-pVTZ calculations indicate that the oxide involves little charge transfer (+1.03e on Ni and -0.03e on O), with more for the sulfide (+0.84e on Ni and +0.16e on S) but less than in either $PtS^+$ or $PdS^+$. Again most of the electron transfers into the 4s orbital on Ni. The electron distribution in the $^4\Sigma^-$ and $^4\Delta$ states is nearly identical, consistent with their similar energies. Notably, in all six diatomics, the d orbital population remains near 9 electrons (varying between 8.70 in $PtO^+$ to 9.07 in $PdS^+$) indicating that the diatomic species correlate diabatically with the $^2D(nd^9)$ ground state of the metal cation.

**Comparison of the characteristics of $PtO^+$ product formation with previous studies**

Fig. 5 overlays the $PtO^+$ cross sections obtained for reactions of $Pt^+$ with $SO_2$, $O_2$, $CO_2$, CO, and NO by aligning the data at the neutral BDEs such that the x-axis becomes "energy (CM) – $D_0$(XO)." This presentation therefore aligns the thresholds for $PtO^+$ production at the same energy: $-D_0(PtO^+) = -3.26$ eV on this scale. (Results for the $SO_2$ reaction system have been scaled down by a factor of 10 to emphasize a more direct comparison of the energy behavior for all five systems.) This direct comparison shows that the total cross sections for the $O_2$, $CO_2$, and $SO_2$ reactions behave very similarly, whereas the $PtO^+$ cross sections for each of these systems (same as the total for $O_2$) are distinct because of competition with other channels: $PtCO^+$ in the case of the $CO_2$ system and $PtSO^+$ for $SO_2$. Further, it can be seen that the $PtO^+$ cross sections increase rapidly from threshold for the $O_2$, $CO_2$, and $SO_2$ reactions and more slowly for CO and NO. These trends are related to the differences in the endothermicities, which are smallest for the $O_2$ reaction, where $D_0(O-O) = 5.12$ eV, slightly larger for $CO_2$ and $SO_2$, where $D_0$(OC-O) – 5.45 eV and $D_0(OS-O) = 5.66$ eV, larger for NO, $D_0$(N-O) = 6.51 eV, and much larger for the CO reaction, $D_0(C-O) = 11.11$ eV. Another contribution to the distinct behavior of the NO and CO systems is competition with $PtN^+ + O$ and $PtC^+ + O$ formation, respectively. Formation of $PtN^+$ has a similar endothermicity as the $PtO^+$ formation and has a similar cross section magnitude. $PtC^+$ formation

is less endothermic than $PtO^+$ + C formation, thereby suppressing the probability of the latter.

## CONCLUSION

The reaction of atomic platinum cations with sulfur dioxide have been studied over a wide range of kinetic energies using guided ion beam tandem mass spectrometry. Three products are formed in endothermic reactions, $PtO^+$ + SO, $PtS^+$ + $O_2$, and $PtSO^+$ + O. The threshold energies for these reactions are evaluated to yield bond dissociation energies for the three ionic products. That for $PtO^+$ agrees well with previous determinations, whereas the measurements for $PtS^+$ and $PtSO^+$ are novel determinations. In all three cases, theory reproduces the experimental thermochemistry reasonably well. The $PtS^+$ molecule has a stronger bond than the isovalent $PtO^+$ species (both of which are found to have $^4\Sigma_{3/2}$ ground electronic states), a result that theory indicates is a consequence of better orbital overlap. This conclusion is also justified by comparing the present results with the other group 9 metal chalcogenide cations. Theory also indicates that the $PtSO^+$ ($^2A'$) ground state is preferred to an inserted $OPtS^+$ species. Finally, the present results are compared directly with the oxidation reactions observed with four other oxidants examined in previous studies, where similar results are obtained once differences in endothermicities and competition with other channels are accounted for.

## SUPPLEMENTARY MATERIAL

See supplementary material for a table of bond lengths, bond angles, vibrational frequencies, and relative energies of the structures in Fig. 4 along with additional species.

## ACKNOWLEDGMENTS

This research is funded by the National Science Foundation under Grant CHE-1954142. The theoretical calculations are expedited by facilities provided by the Center for High Performance Computing (CHPC) at the University of Utah. Drs. Richard M Cox and JungSoo Kim are thanked for collecting the data.

## DATA AVAILABILITY

The data that support the findings of this study are available within the article and its supplementary material.

## AUTHOR INFORMATION

Corresponding Author

P. B. Armentrout − Department of Chemistry, University of Utah, Salt Lake City, Utah 84112, United States; orcid.org/0000-0003-2953-6039; Email: armentrout@chem.utah.edu

## REFERENCES

[1] D. P. Rall,"Review of the health effects of sulfur oxides", Environ. Health Perspect. **8**, 97 (1974).
[2] J. Q. Koenig, "Health Effects of Sulfur Oxides: Sulfur Dioxide and Sulfuric Acid", in *Health Effects of Ambient Air Pollution: How safe is the air we breathe?*, edited by J. Q. Koenig, Springer US, Boston, MA, (2000), pp. 99.
[3] D. J. Donaldson, and J. Kroll,"Gas-phase hydrolysis of triplet SO2: A possible direct route to atmospheric acid formation", Scientific Reports **6**, 30000 (2016).
[4] P. G. Menon,"Diagnosis of Industrial Catalyst Deactivation by Surface Characterization Techniques", Chem. Rev. **94**, 1021 (1994).
[5] W. Aas, A. Mortier, V. Bowersox, R. Cherian, G. Faluvegi, H. Fagerli, J. Hand, Z. Klimont, G.-L. Corinne, C. Lehmann, C. Lund Myhre, G. Myhre, D. Olivié, K. Sato, J. Quaas, R. Pasumarti, S. Michael, D. Shindell, R. Skeie, and X. Xu,"Global and regional trends of atmospheric sulfur", Scientific Reports **9**, 953 (2019).
[6] S. K. Gangwal, W. J. McMichael, and T. P. Dorchak,"The direct sulfur recovery process", Environ. Prog. **10**, 186 (1991).
[7] J. W. Portzer, B. S. Turk, and S. K. Gangwal, 1996).
[8] R. R. Ryan, G. J. Kubas, D. C. Moody, and P. G. Eller, in *Inorg. Chem.* (Springer Berlin Heidelberg, Berlin, Heidelberg, 1981), pp. 47.
[9] G. J. Kubas,"Chemical Transformations and Facile Disproportionation of Sulfur Dioxide on Transition Metal Complexes", Acc. Chem. Res. **27**, 183 (1994).
[10] W. A. Schenk,"The coordination chemistry of small sulfur-containing molecules: a personal perspective", Dalton Trans. **40**, 1209 (2011).
[11] S.-G. He, Y. Xie, F. Dong, S. Heinbuch, E. Jakubikova, J. J. Rocca, and E. R. Bernstein,"Reactions of sulfur dioxide with neutral vanadium oxide clusters in the gas phase. II. Experimental study employing single-photon ionization", The journal of physical chemistry. A **112 44**, 11067 (2008).
[12] Z.-X. Zhou, L. N. Wang, Z.-Y. Li, S.-G. He, and T.-M. Ma,"Oxidation of $SO_2$ to $SO_3$ by Cerium Oxide Cluster Cations $Ce_2O_4^+$ and $Ce_3O_6^+$", J. Phys. Chem. A **120**, 3843 (2016).

[13] J. M. Mercero, E. Rezabal, J. M. Ugalde, T. Weiske, and J. Li,"Experiment and Theory Clarify: $Sc^+$ Receives One Oxygen Atom from $SO_2$ to Form $ScO^+$, which Proves to be a Catalyst for the Hidden Oxygen-Exchange with $SO_2$", ChemPhysChem **23**, e202100773 (2021).
[14] J. Kim, and P. B. Armentrout,"Guided Ion Beam Tandem Mass Spectrometry and Theoretical Study of $SO_2$ Activated by $Os^+$ ", J. Phys. Chem. A **124**, 6629 (2020).
[15] J. Kim, R. M. Cox, and P. B. Armentrout,"Thermochemical Studies of Reactions of $Re^+$ with $SO_2$ Using Guided Ion Beam Experiments and Theory", Phys. Chem. Chem. Phys. **22**, 3191 (2020).
[16] J. Kim, and P. B. Armentrout,"Thermochemistry of $Ir^+ + SO_2$ Reaction using Guided Ion Beam Tandem Mass Spectrometry and Theory", J. Chem. Phys. **154**, 124302 (2021).
[17] P. B. Armentrout,"The Bond Energy of $ReO^+$: Guided Ion-Beam and Theoretical Studies of the Reaction of $Re^+$ ($^7S$) with $O_2$", J. Chem. Phys. **139**, 084305 (2013).
[18] C. S. Hinton, M. Citir, and P. B. Armentrout,"Guided Ion-Beam and Theoretical Studies of the Reaction of $Os^+$ ($^6D$) with $O_2$: Adiabatic and Nonadiabatic Behavior", Int. J. Mass Spectrom. **354-355**, 87 (2013).
[19] P. B. Armentrout, and F.-X. Li,"Bond Energy of $IrO^+$: Guided Ion-Beam and Theoretical Studies of the Reaction of $Ir^+$ ($^5F$) with $O_2$", J. Phys. Chem. A **117**, 7754 (2013).
[20] C. S. Hinton, F.-X. Li, and P. B. Armentrout,"Reactions of $Hf^+$, $Ta^+$, and $W^+$ with $O_2$ and CO: Metal Carbide and Metal Oxide Cation Bond Energies", Int. J. Mass Spectrom. **280**, 226 (2009).
[21] X.-G. Zhang, and P. B. Armentrout,"Activation of $O_2$, CO, and $CO_2$ by $Pt^+$: The Thermochemistry of $PtO^+$", J. Phys. Chem. A **107**, 8904 (2003).
[22] F.-X. Li, K. Gorham, and P. B. Armentrout,"Oxidation of Atomic Gold Ions: Thermochemistry for the Activation of $O_2$ and $N_2O$ by $Au^+$ ($^1S_0$ and $^3D$)", J. Phys. Chem. A **114**, 11043 (2010).
[23] X.-G. Zhang, and P. B. Armentrout,"Activation of $O_2$ and $CO_2$ by $PtO^+$: The Thermochemistry of $PtO_2^+$", J. Phys. Chem. A **107**, 8915 (2003).
[24] J. J. Sorensen, E. Tieu, and M. D. Morse,"Bond Dissociation Energies of the Diatomic Late Transition Metal Sulfides: RuS, OsS, CoS, RhS, IrS, and PtS", J. Chem. Phys. **152**, 244305 (2020).
[25] S. K. Loh, D. A. Hales, L. Lian, and P. B. Armentrout,"Collision-Induced Dissociation of $Fe_n^+$ ($n$ = 2 - 10) with Xe: Ionic and Neutral Iron Cluster Binding Energies", J. Chem. Phys. **90**, 5466 (1989).
[26] R. H. Schultz, and P. B. Armentrout,"Reactions of $N_4^+$ with Rare Gases from Thermal to 10 eV c.m.: Collision-Induced Dissociation, Charge Transfer, and Ligand Exchange", Int. J. Mass Spectrom. Ion Processes **107**, 29 (1991).
[27] D. E. Clemmer, Y.-M. Chen, F. A. Khan, and P. B. Armentrout,"State-Specific Reactions of $Fe^+$($a^6D$, $a^4F$) with $D_2O$ and Reactions of $FeO^+$ with $D_2$", J. Phys. Chem. **98**, 6522 (1994).
[28] C. L. Haynes, and P. B. Armentrout,"Thermochemistry and Structures of $CoC_3H_6^+$: Metallacycle and Metal-Alkene Isomers", Organomet. **13**, 3480 (1994).
[29] B. L. Kickel, and P. B. Armentrout,"Guided Ion Beam Studies of the Reactions of Group 3 Metal Ions ($Sc^+$, $Y^+$, $La^+$, and $Lu^+$) with Silane. Electronic State Effects, Comparison to Reactions with Methane, and $M^+$-$SiH_x$ (x = 0 - 3) Bond Energies", J. Am. Chem. Soc. **117**, 4057 (1995).
[30] B. L. Kickel, and P. B. Armentrout,"Reactions of $Fe^+$, $Co^+$ and $Ni^+$ with Silane. Electronic State Effects, Comparison to Reactions with Methane, and $M^+$-$SiH_x$ ($x$ = 0 - 3) Bond Energies", J. Am. Chem. Soc. **117**, 764 (1995).

[31] Y.-M. Chen, J. L. Elkind, and P. B. Armentrout,"Reactions of $Ru^+$, $Rh^+$, $Pd^+$, and $Ag^+$ with $H_2$, HD and $D_2$", J. Phys. Chem. **99**, 10438 (1995).
[32] M. R. Sievers, Y.-M. Chen, J. L. Elkind, and P. B. Armentrout,"Reactions of $Y^+$, $Zr^+$, $Nb^+$, and $Mo^+$ with $H_2$, HD, and $D_2$", J. Phys. Chem. **100**, 54 (1996).
[33] F.-X. Li, X.-G. Zhang, and P. B. Armentrout,"The Most Reactive Third-row Transition Metal: Guided Ion Beam and Theoretical Studies of the Activation of Methane by $Ir^+$", Int. J. Mass Spectrom. **255/256**, 279 (2006).
[34] J. Kim, R. M. Cox, and P. B. Armentrout,"Guided Ion Beam and Theoretical Studies of the Reactions of $Re^+$, $Os^+$, and $Ir^+$ with CO", J. Chem. Phys. **145**, 194305 (2016).
[35] T. Su, and W. J. Chesnavich,"Parameterization of the Ion-polar Molecule Collision Rate Constant by Trajectory Calculations", J. Chem. Phys. **76**, 5183 (1982).
[36] E. Teloy, and D. Gerlich,"Integral Cross Sections for Ion-Molecule Reactions. 1. The Guided Beam Technique", Chem. Phys. **4**, 417 (1974).
[37] D. Gerlich, "Inhomogeneous rf Fields: A Versatile Tool for the Study of Processes with Slow Ions", *Adv. Chem. Phys.***82**, 1 (1992).
[38] N. R. Daly,"Scintillation Type Mass Spectrometer Ion Detector", Rev. Sci. Instrum. **31**, 264 (1960).
[39] K. M. Ervin, and P. B. Armentrout,"Translational Energy Dependence of $Ar^+ + XY \rightarrow ArX^+ + Y$ ($XY = H_2$, $D_2$, HD) from Thermal to 30 eV c.m.", J. Chem. Phys. **83**, 166 (1985).
[40] P. J. Chantry,"Doppler Broadening in Beam Experiments", J. Chem. Phys. **55**, 2746 (1971).
[41] C. Lifshitz, R. L. C. Wu, T. O. Tiernan, and D. T. Terwilliger,"Negative Ion-molecule Reactions of Ozone and Their Implications on the Thermochemistry of $O_3^-$", J. Chem. Phys. **68**, 247 (1978).
[42] M. E. Weber, J. L. Elkind, and P. B. Armentrout,"Kinetic Energy Dependence of $Al^+ + O_2 \rightarrow AlO^+ + O$", J. Chem. Phys. **84**, 1521 (1986).
[43] R. D. Johnson III, in *NIST Standard Reference Database Number 101, Release 19*, edited by D. J. Russell, III (NIST Computational Chemistry Comparison and Benchmark Database, 2018).
[44] P. B. Armentrout, and J. Simons,"Understanding Heterolytic Bond Cleavage", J. Am. Chem. Soc. **114**, 8627 (1992).
[45] M. J. Frisch, G. W. Trucks, H. B. Schlegel, G. E. Scuseria, M. A. Robb, J. R. Cheeseman, G. Scalmani, V. Barone, G. A. Petersson, H. Nakatsuji, X. Li, M. Caricato, A. V. Marenich, J. Bloino, B. G. Janesko, R. Gomperts, B. Mennucci, H. P. Hratchian, J. V. Ortiz, A. F. Izmaylov, J. L. Sonnenberg, D. Williams-Young, F. Ding, F. Lipparini, F. Egidi, J. Goings, B. Peng, A. Petrone, T. Henderson, D. Ranasinghe, V. G. Zakrzewski, J. Gao, N. Rega, G. Zheng, W. Liang, M. Hada, M. Ehara, K. Toyota, R. Fukuda, J. Hasegawa, M. Ishida, T. Nakajima, Y. Honda, O. Kitao, H. Nakai, T. Vreven, K. Throssell, J. J. A. Montgomery, J. E. Peralta, F. Ogliaro, M. J. Bearpark, J. J. Heyd, E. N. Brothers, K. N. Kudin, V. N. Staroverov, T. A. Keith, R. Kobayashi, J. Normand, K. Raghavachari, A. P. Rendell, J. C. Burant, S. S. Iyengar, J. Tomasi, M. Cossi, J. M. Millam, M. Klene, C. Adamo, R. Cammi, J. W. Ochterski, R. L. Martin, K. Morokuma, O. Farkas, J. B. Foresman, and D. J. Fox,"Gaussian 16, Revision A.03", (2016).
[46] A. D. Becke,"Density-functional Thermochemistry. III. The Role of Exact Exchange", J. Chem. Phys. **98**, 5648 (1993).
[47] C. Lee, W. Yang, and R. G. Parr,"Development of the Colle-Salvetti Correlation-Energy Formula into a Functional of the Electron Density", Phys. Rev. B **37**, 785 (1988).

[48] K. Raghavachari, G. W. Trucks, J. A. Pople, and M. Head-Gordon,"A Fifth-order Perturbation Comparison of Electron Correlation Theories", Chem. Phys. Lett. **157**, 479 (1989).
[49] R. J. Bartlett, J. D. Watts, S. A. Kucharski, and J. Noga,"Non-iterative Fifth-order Triple and Quadruple Excitation Energy Corrections in Correlated Methods", Chem. Phys. Lett. **165**, 513 (1990).
[50] G. E. Scuseria, and T. J. Lee,"Comparison of Coupled-cluster Methods Which Include the Effects of Connected Triple Excitations", J. Chem. Phys. **93**, 5851 (1990).
[51] T. D. Crawford, and J. F. Stanton,"Investigation of an Asymmetric Triple-Excitation Correction for Coupled-Cluster Energies", Int. J. Quantum Chem. **70**, 601 (1998).
[52] M. M. Armentrout, F.-X. Li, and P. B. Armentrout,"Is Spin Conserved in Heavy Metal Systems? Experimental and Theoretical Studies of the Reaction of $Re^+$ with Methane", J. Phys. Chem. A **108**, 9660 (2004).
[53] P. B. Armentrout, L. Parke, C. Hinton, and M. Citir,"Activation of Methane by $Os^+$: Guided Ion Beam and Theoretical Studies", ChemPlusChem **78**, 1157 (2013).
[54] D. Andrae, U. Haeussermann, M. Dolg, H. Stoll, and H. Preuss,"Energy-adjusted Ab Initio Pseudopotentials for the Second and Third Row Transition Elements", Theor. Chim. Acta **77**, 123 (1990).
[55] F. Weigend, and R. Ahlrichs,"Balanced Basis Sets of Split Valence, Triple Zeta Valence and Quadruple Zeta Valence Quality for H to Rn: Design and Assessment of Accuracy", Phys. Chem. Chem. Phys. **7**, 3297 (2005).
[56] D. Figgen, K. A. Peterson, M. Dolg, and H. Stoll,"Energy-consistent Pseudopotentials and Correlation Consistent Basis Sets for the 5d Elements Hf-Pt", J. Chem. Phys. **130**, 164108 (2009).
[57] D. Feller,"The Role of Databases in Support of Computational Chemistry Calculations", J. Comput. Chem. **17**, 1571 (1996).
[58] K. L. Schuchardt, B. T. Didier, T. Elsethagen, L. Sun, V. Gurumoorthi, J. Chase, J. Li, and T. L. Windus,"Basis Set Exchange: A Community Database for Computational Sciences", J. Chem. Inf. Model. **47**, 1045 (2007).
[59] A. Karton, and J. M. L. Martin,"Comment on: “Estimating the Hartree–Fock limit from finite basis set calculations” [Jensen F (2005) Theor Chem Acc 113:267]", Theor. Chem. Acct. **115**, 330 (2006).
[60] J. M. L. Martin,"Ab initio Total Atomization Energies of Small Molecules - Towards the Basis Set Limit", Chem. Phys. Lett. **259**, 669 (1996).
[61] T. J. Lee, and P. R. Taylor,"A diagnostic for determining the quality of single-reference electron correlation methods", Int. J. Quantum Chem. **36**, 199 (1989).
[62] J. C. Rienstra-Kiracofe, W. D. Allen, and H. F. Schaefer,"The C2H5 + O2 Reaction Mechanism: High-Level ab Initio Characterizations", J. Phys. Chem. A **104**, 9823 (2000).
[63] X.-G. Zhang, and P. B. Armentrout,"Guided Ion Beam Study of Potential Energy Surfaces for Platinum Interactions with Nitrogen Oxides", Eur. J. Mass Spectrom. **10**, 963 (2004).
[64] C. J. Thompson, K. L. Stringer, M. McWilliams, and R. B. Metz,"Electronic spectroscopy of predissociative states of platinum oxide cation", Chem. Phys. Lett. **376**, 588 (2003).
[65] M. Citir, R. B. Metz, L. Belau, and M. Ahmed,"Direct Determination of the Ionization Energies of PtC, PtO, and PtO with VUV Radiation", J. Phys. Chem. A **112**, 9584 (2008).
[66] W. J. Chesnavich, and M. T. Bowers,"Statistical Phase Space Theory of Polyatomic Systems: Rigorous Energy and Angular Momentum Conservation in Reactions Involving Symmetric Polyatomic Species", J. Chem. Phys. **66**, 2306 (1977).

[67] D. A. Webb, and W. J. Chesnavich,"Multiple Transition State Models for the Reactions $C^+$ ($D_2$,D) $CD^+$ and $C^+$ ($H_2$,H) $CH^+$", J. Phys. Chem. **87**, 3791 (1983).
[68] K. M. Ervin, and P. B. Armentrout,"$C^+(^2P)$ + $H_2(D_2,HD)$ → $CH^+(CD^+)$ + H(D) II. Statistical Phase Space Theory", J. Chem. Phys. **84**, 6750 (1986).
[69] A. Kramida, Y. Ralchenko, J. Reader, and N. A. Team, (National Institute of Standards and Technology, Gaithersburg, MD., 2012).
[70] M. Brönstrup, D. Schröder, I. Kretzschmar, H. Schwarz, and J. N. Harvey,"Platinum Dioxide Cation: Easy to Generate Experimentally but Difficult to Describe Theoretically", J. Am. Chem. Soc. **123**, 142 (2001).
[71] C. Heinemann, W. Koch, and H. Schwarz,"An approximate method for treating spin-orbit effects in platinum", Chem. Phys. Lett. **245**, 509 (1995).
[72] H. Lefebvre-Brion, and R. W. Field, *The Spectra and Dynamics of Diatomic Molecules* (Elsevier, Amsterdam, 2004),
[73] M. A. Garcia, and M. D. Morse,"Resonant Two-photon Ionization Spectroscopy of Jet-cooled OsN: 520–418 nm", J. Chem. Phys. **135**, 114304 (2011).
[74] R. G. Wilson, and G. R. Brewer, *Ion Beams with Applications to Ion Implantation* (Wiley, New York, 1973),
[75] J. P. Foster, and F. Weinhold,"Natural Hybrid Orbitals", J. Am. Chem. Soc. **102**, 7211 (1980).
[76] E. D. Glendening, A. E. Reed, J. E. Carpenter, and F. Weinhold,"NBO Version 3.1", (2003).
[77] Y.-M. Chen, and P. B. Armentrout,"Kinetic Energy Dependence of the Reactions of $Ru^+$, $Rh^+$, $Pd^+$, and $Ag^+$ with $O_2$", J. Chem. Phys. **103**, 618 (1995).
[78] P. B. Armentrout, and I. Kretzschmar,"Experimental and Theoretical Studies of the Reaction of $Pd^+$ with $CS_2$ in the Gas-phase: Thermochemistry of $PdS^+$ and $PdCS^+$", Inorg. Chem. **48**, 10371 (2009).
[79] E. A. Carter, and W. A. Goddard,"Relationships between bond energies in coordinatively unsaturated and coordinatively saturated transition-metal complexes: a quantitative guide for single, double, and triple bonds", J. Phys. Chem **92**, 5679 (1988).
[80] S. P. Lockwood, T. Chunga, and R. B. Metz,"Bonding, Thermodynamics, and Dissociation Dynamics of $NiO^+$ and $NiS^+$ Determined by Photofragment Imaging and Theory", J. Phys. Chem. A **125**, 7425 (2021).
[81] E. R. Fisher, J. L. Elkind, D. E. Clemmer, R. Georgiadis, S. K. Loh, N. Aristov, L. S. Sunderlin, and P. B. Armentrout,"Reactions of Fourth Period Metal Ions ($Ca^+$ - $Zn^+$) with $O_2$: Metal Oxide Ion Bond Energies", J. Chem. Phys. **93**, 2676 (1990).
[82] E. R. Fisher, and P. B. Armentrout,"Reactions of $Co^+$, $Ni^+$, and $Cu^+$ with Cyclopropane and Ethylene Oxide: Metal Methylidene Ion Bond Energies", J. Phys. Chem. **94**, 1674 (1990).
[83] C. Rue, P. B. Armentrout, I. Kretzschmar, D. Schröder, and H. Schwarz,"Guided Ion Beam Studies of the Reactions of $Ni^+$, $Cu^+$, and $Zn^+$ with $CS_2$ and COS", J. Phys. Chem. A **106**, 9788 (2002).
[84] C. N. Sakellaris, and A. Mavridis,"First principles exploration of NiO and its ions NiO+ and NiO−", J. Chem. Phys. **138**, 054308 (2013).
[85] M. Pavlov, M. R. A. Blomberg, P. E. M. Siegbahn, R. Wesendrup, C. Heinemann, and H. Schwarz,"$Pt^+$-Catalyzed Oxidation of Methane: Theory and Experiment", J. Phys. Chem. A **101**, 1567 (1997).

**Table I.** Experimental and theoretical BDEs (eV) at 0 K of the reaction products.

| Species | Experimental [a] | | | Theoretical [b] | | | |
|---|---|---|---|---|---|---|---|
| | Current | Literature | State | B3LYP/ def2-T | CCSD(T)/ def2-Q | CCSD(T)/ CBS | Literature |
| $Pt^+$–O | 3.14 (0.11) | 3.26 (0.04)[c] | $^4\Sigma_{3/2}^-$ | 3.14 | 3.04 | 3.10 | 3.14[e] |
| | | ≤ 3.164 [d] | | | | | 3.14[f] |
| | | | | | | | 3.33[g] |
| | | | | | | | 2.97[h] |
| $Pt^+$–S | 3.68 (0.31) | | $^4\Sigma_{3/2}^-$ | 3.68 | 3.62 | 3.70 | |
| $OPt^+$–O | | 3.06 (0.07)[i] | $^2\Sigma_g^+$ | 2.56 | 3.28 | 3.47 | 3.50[f] |
| | | | | | | | 3.62[g] |
| | | | | | | | 2.64[i] |
| $Pt^+$–$O_2$ | | 0.67 (0.05)[i] | $^2A''$ | 0.54 | 0.46 | 0.63 | 0.77[f] |
| | | | | | | | 0.89[g] |
| | | | | | | | 0.52[j] |
| $Pt^+$–SO | 3.03 (0.12) | | $^2A'$ | 2.63 | 2.87 | 2.96 | |

[a] Uncertainties in parentheses are one standard deviation. [b] S.O. corrected. See text. Def2-X = def2-XZVPPD, CBS = complete basis set extrapolation (see text). [c] Refs. [21] and [63]. [d] Ref. [64]. [e] Ref. [85] (PCI-80). [f] Ref. [70] (MR-QDPT). [g] Ref. [70] (CASPT2). [h] Ref. [21] (B3LYP). [i] Ref. [23] (B3LYP).

**Table II.** Parameters for modeling cross sections of reactions (6) – (9) with Eq. (1) and $P_D$. [a]

| Species | Energy Range (eV) | $\sigma_0$ | $n$ | $E_0$ (eV) | $p$ | $E_D$ (eV) |
|---|---|---|---|---|---|---|
| Total ($PtO^+$) | 0 – 9 | 8.0 ± 2.1 | 1.8 ± 0.1 | 2.52 ± 0.11 | 3 | 6.11 ± 0.10 |
| $PtSO^+$ | 0 – 9 | 3.0 ± 1.0 | 2.4 ± 0.2 | 2.63 ± 0.12 | 4 | 6.08 ± 0.08 |
| $PtO_2^+$/$PtS^+$ | 0 – 6 | 0.012 ± 0.004 | 2.3 | 2.2 | 2 | 5.90[b] |
| $PtS^+$ | 7 – 11 | 0.36 ± 0.16 | 1.5 ± 0.3 | 7.34 ± 0.31 | | |

[a] Uncertainties are one standard deviation. Parameters are defined in the text. [b] Set equal to $D_0(S\text{-}O_2)$.

**Table III.** Bond lengths (r, Å), vibrational frequencies ($\omega_e$, $cm^{-1}$), and bond (*relative*) energies (eV) calculated at various levels of theory for the lowest energy states of $PtO^+$.

| State | Level | Basis Set | *r*(Pt-O) | $\omega_e$ [a] | E ($E_h$) | $D_0$ / $E_{rel}$ [b] |
|---|---|---|---|---|---|---|
| $^4\Sigma_{3/2}^-$ | B3LYP | def2-TZVPPD | 1.736 | 813 | -194.194588 | 3.14 |
| | CCSD(T) | def2-TZVPPD | 1.737 | 818 | -193.692038 | 2.92 |
| | CCSD(T) | def2-QZVPPD | | | -193.784582 | 3.04 |
| | B3LYP | aug-cc-pVTZ | 1.731 | 825 | -194.307980 | 3.24 |
| | CCSD(T) | aug-cc-pVTZ | 1.730 | 831 | -193.949507 | 3.04 |
| | CCSD(T) | aug-cc-pVQZ | | | -194.018096 | 3.08 |
| | CCSD(T) | aug-cc-pV5Z | | | -194.046224 | 3.09 |
| | CCSD(T) | CBS [c] | | | -194.068480 | 3.10 |
| $^2\Sigma_{1/2}^-$ | B3LYP | def2-TZVPPD | 1.731 | 839 | -194.176285 | *0.54* |
| | CCSD(T) | def2-TZVPPD | 1.723 | 875 | -193.671190 | *0.61* |
| | CCSD(T) | def2-QZVPPD | | | -193.763616 | *0.61* |
| | B3LYP | aug-cc-pVTZ | 1.726 | 849 | -194.289855 | *0.54* |
| | CCSD(T) | aug-cc-pVTZ | 1.715 | 890 | -193.928366 | *0.62* |
| | CCSD(T) | aug-cc-pVQZ | | | -194.000544 | *0.62* |
| | CCSD(T) | aug-cc-pV5Z | | | -194.028762 | *0.62* |
| | CCSD(T) | CBS [c] | | | -194.051073 | *0.62* |
| $^4\Delta_{7/2}$ | B3LYP | def2-TZVPPD | 1.814 | 679 | -194.158100 | *0.71* |
| | CCSD(T) | def2-TZVPPD | 1.809 | 703 | -193.671191 | *0.68* |
| | CCSD(T) | def2-QZVPPD | | | -193.763616 | *0.70* |
| | B3LYP | aug-cc-pVTZ | 1.805 | 695 | -194.271668 | *0.66* |
| | CCSD(T) | aug-cc-pVTZ [d] | 1.797 | 722 | -193.913161 | *0.66* |
| $^2\Pi_{1/2}$ | B3LYP | def2-TZVPPD | 1.699 | 810 | -194.149027 | *1.18* |
| | CCSD(T) | def2-TZVPPD | 1.704 | 865 | -193.655119 | *0.95* |
| | CCSD(T) | def2-QZVPPD | | | -193.748064 | *0.94* |
| | B3LYP | aug-cc-pVTZ | 1.692 | 850 | -194.263913 | *1.14* |
| | CCSD(T) | aug-cc-pVTZ | 1.694 | 876 | -193.914503 | *0.89* |
| | CCSD(T) | aug-cc-pVQZ | | | -193.982566 | *0.91* |
| | CCSD(T) | aug-cc-pV5Z | | | -194.010412 | *0.92* |
| | CCSD(T) | CBS [c] | | | -194.032428 | *0.92* |

[a] Vibrational frequencies unscaled. [b] 0 K bond dissociation energy (normal font) or energy relative to ground state (*italic font*). Values include S.O. corrections for $^4\Sigma_{3/2}^-$, $^2\Sigma_{1/2}^-$, $^2\Pi_{1/2}$, and $^4\Delta_{7/2}$ states of 0.20, 0.16, 0.26, and 0.52 eV, respectively, and BDE values include the S.O. corrections for $Pt^+$ ($^2D_{5/2}$) and O($^3P_2$) of 0.418 and 0.010 eV. [c] Complete basis set extrapolated value from X = Q and 5 (see text). [d] Calculations with larger basis sets would not converge.

**Table IV.** Bond lengths (r, Å), vibrational frequencies ($\omega_e$, $cm^{-1}$), and bond (*relative*) energies (eV) calculated at various levels of theory for the lowest energy states of $PtS^+$.

| State | Level | Basis Set | *r*(Pt-S) | $\omega_e$ [a] | E ($E_h$) | $D_0$ / $E_{rel}$ [b] |
|---|---|---|---|---|---|---|
| $^4\Sigma_{3/2}^-$ | B3LYP | def2-TZVPPD | 2.093 | 469 | -517.250391 | 3.68 |
| | CCSD(T) | def2-TZVPPD | 2.078 | 490 | -516.380403 | 3.44 |
| | CCSD(T) | def2-QZVPPD | | | -516.479893 | 3.62 |
| | B3LYP | aug-cc-pVTZ | 2.088 | 474 | -517.373587 | 3.74 |
| | CCSD(T) | aug-cc-pVTZ | 2.073 | 495 | -516.644609 | 3.57 |
| | CCSD(T) | aug-cc-pVQZ | | | -516.711558 | 3.66 |
| | CCSD(T) | aug-cc-pV5Z | | | -516.738833 | 3.69 |
| | CCSD(T) | CBS [c] | | | -516.760712 | 3.70 |
| $^2\Pi_{1/2}$ | B3LYP | def2-TZVPPD | 2.012 | 546 | -517.235078 | *0.36* |
| | CCSD(T) | def2-TZVPPD | 2.023 | 516 | -516.373615 | *0.12* |
| | CCSD(T) | def2-QZVPPD | | | -516.474772 | *0.08* |
| | B3LYP | aug-cc-pVTZ | 2.009 | 552 | -517.359294 | *0.33* |
| | CCSD(T) | aug-cc-pVTZ | 2.015 | 529 | -516.640211 | *0.06* |
| | CCSD(T) | aug-cc-pVQZ | | | -516.741467 | *0.05* |
| | CCSD(T) | aug-cc-pV5Z | | | -516.741993 | *0.05* |
| | CCSD(T) | CBS [c] | | | -516.756528 | *0.05* |
| $^4\Delta_{7/2}$ | B3LYP | def2-TZVPPD | 2.145 | 433 | -517.232783 | *0.15* |
| | CCSD(T) | def2-TZVPPD | 2.123 | 456 | -516.363418 | *0.14* |
| | CCSD(T) | def2-QZVPPD | | | -516.462428 | *0.15* |
| | B3LYP | aug-cc-pVTZ | 2.138 | 439 | -517.356516 | *0.14* |
| | CCSD(T) | aug-cc-pVTZ | 2.123 | 456 | -516.628787 | *0.11* |
| | CCSD(T) | aug-cc-pVQZ | | | -516.694244 | *0.15* |
| | CCSD(T) | aug-cc-pV5Z | | | -516.720929 | *0.16* |
| | CCSD(T) | CBS [c] | | | -516.742306 | *0.18* |
| $^2\Sigma_{1/2}^-$ | B3LYP | def2-TZVPPD | 2.092 | 473 | -517.238262 | *0.37* |
| | CCSD(T) | def2-TZVPPD | 2.080 | 500 | -516.365509 | *0.45* |
| | CCSD(T) | def2-QZVPPD | | | -516.465314 | *0.44* |
| | B3LYP | aug-cc-pVTZ | 2.088 | 478 | -517.361533 | *0.47* |
| | CCSD(T) | aug-cc-pVTZ | 2.071 | 541 | -516.629838 | *0.44* |
| | CCSD(T) | aug-cc-pVQZ | | | -516.696974 | *0.44* |
| | CCSD(T) | aug-cc-pV5Z | | | -516.724307 | *0.44* |
| | CCSD(T) | CBS [c] | | | -516.746222 | *0.44* |

[a] Vibrational frequencies unscaled. [b] 0 K bond dissociation energy (normal font) or energy relative to ground state (*italic font*). Values include S.O. corrections for $^4\Sigma_{3/2}^-$,$^2\Pi_{1/2}$, $^4\Delta_{7/2}$, and $^2\Sigma_{1/2}^-$ states of 0.20, 0.26, 0.52, and 0.16 eV, respectively, and BDE values include the S.O. corrections for $Pt^+$ ($^2D_{5/2}$) and S ($^3P_2$) of 0.418 and 0.024 eV. [c] Complete basis set extrapolated value from X = Q and 5 (see text).

**Table V.** Bond lengths (r, Å), bond angles (°), vibrational frequencies ($\omega_e$, $cm^{-1}$), and bond (*relative*) energies (eV) calculated at various levels of theory of $PtO_2^+$.

| State | Level | Basis Set | r(Pt-O) | ∠OPtO | $\omega_e$ [a] | E ($E_h$) | $D_0$ / $E_{rel}$ (eV) [b] |
|---|---|---|---|---|---|---|---|
| $OPtO^+$ ($^2\Sigma_g^+$) | B3LYP | def2-TZVPPD | 1.685 | 177.5 | 13, 1008, 1022 | -269.396139 | 2.57/0.45 |
| | CCSD(T) | def2-TZVPPD | 1.686 | 180.0 | 84 (2), 863, 1072 | -268.799013 | 3.22/1.31 |
| | CCSD(T) | def2-QZVPPD | | | | -268.910218 | 3.29/1.36 |
| | B3LYP | aug-cc-pVTZ | 1.680 | 180.0 | 50 (2), 1016, 1036 | -269.515950 | 2.79/0.79 |
| | CCSD(T) | aug-cc-pVTZ | 1.683 | 180.0 | 42, 68, 882, 1092 | -269.066674 | 3.38/1.56 |
| | CCSD(T) | aug-cc-pVQZ | | | | -269.152002 | 3.44/1.53 |
| | CCSD(T) | aug-cc-pV5Z | | | | -269.185331 | 3.46/1.51 |
| | CCSD(T) | CBS[c] | | | | -269.211318 | 3.47/1.50 |
| $PtOO^+$ ($^2A''$) | B3LYP | def2-TZVPPD | 2.005, 2.779 | 22.8 | 158, 397, 1485 | -269.399998 | *-0.11* |
| | CCSD(T) | def2-TZVPPD | | | | -268.765762 | *0.90* |
| | CCSD(T) | def2-QZVPPD | | | | -268.877181 | *0.90* |
| | B3LYP | aug-cc-pVTZ | 1.991, 2.760 | 23.2 | 153, 406, 1466 | -269.508743 | *0.20* |
| $^2A_2$ | CCSD(T) | aug-cc-pVTZ | 2.003 (2) | 36.7 | 495, 583, 1450 | -269.038125 | *0.80* |
| | CCSD(T) | aug-cc-pVQZ | | | | -269.119191 | *0.92* |
| | CCSD(T) | aug-cc-pV5Z | | | | -269.1534358 | *0.90* |
| | CCSD(T) | CBS[c] | | | | -269.180155[c] | *0.88* |

[a] Vibrational frequencies are unscaled. [b] $OPt^+$-O/$Pt^+$-$O_2$ BDEs (standard font) or excitation energies (*italic font*) corrected for S.O. splitting of $Pt^+$, $PtO^+$, and O. Uncorrected BDEs are 0.21/0.418 eV higher. [c] Complete basis set extrapolated value from Q and 5 results (see text).

**Table VI.** Bond lengths (r, Å), bond angles (°), vibrational frequencies ($\omega_e$, $cm^{-1}$) and bond (relative) energies (eV) calculated at B3LYP/def2-TZVPPD level of various states of $PtSO^+$.

| Molecules | State | r(Pt-S) | r(Pt-O) | r(S-O) | ∠SPtO | $\omega_e$ [a] | E ($E_h$) | $D_0$/*$E_{rel}$* [b] |
|---|---|---|---|---|---|---|---|---|
| $PtSO^+$ | $^2A'$ | 2.059 | 3.024 | 1.437 | 24.7 | 234, 438, 1285 | -592.517174 | 2.63 |
| $Pt^+(OS)$ | $^2A''$ | 2.184 | 2.067 | 1.536 | 42.2 | 305, 378, 1015 | -592.495234 | *0.58* |
| $PtSO^+$ | $^4A'$ | 2.274 | 3.032 | 1.478 | 28.0 | 156, 314, 1117 | -592.475836 | *1.10* |
| $OPtS^+$ | $^2A'$ | 2.083 | 1.740 | 3.422 | 126.8 | 130, 470, 800 | -592.447115 | *1.87* |
| $OPtS^+$ | $^4A'$ | 2.119 | 1.761 | 3.203 | 110.9 | 189, 441, 774 | -592.443952 | *1.96* |

[a] Vibrational frequencies are unscaled.

[b] Bond dissociation energy (standard font) for $Pt^+$-SO including a S.O. correction of 0.418 eV or energy relative to ground state (italic font).

**Table VII.** Bond lengths (r, Å), bond angles (°), vibrational frequencies ($\omega_e$, $cm^{-1}$), and bond (*relative)* energies (eV) calculated at B3LYP and CCSD(T)//B3LYP levels of theory of $PtSO^+$.

| State | Level | Basis Set | r(Pt-S) | r(Pt-O) | r(S-O) | ∠OPtS | $\omega_e$ [a] | E ($E_h$) | $D_0$ / $E_{rel}$ (eV) [b] |
|---|---|---|---|---|---|---|---|---|---|
| $PtSO^+$ $^2A'$ | B3LYP | def2-TZVPPD | 2.059 | 3.024 | 1.437 | 24.7 | 234, 438, 1285 | -592.517174 | 2.63 |
| | CCSD(T) | def2-TZVPPD | 2.036 | 3.022 | 1.444 | 24.6 | 225, 464, 1262 | -591.526465 | 2.68 |
| | CCSD(T) | def2-QZVPPD | | | | | | -591.648532 | 2.87 |
| | B3LYP | aug-cc-pVTZ | 2.056 | 3.024 | 1.439 | 24.7 | 233, 440, 1282 | -592.637712 | 2.67 |
| | CCSD(T) | aug-cc-pVTZ | | | | | | -591.795035 | 2.77 |
| | CCSD(T) | aug-cc-pVQZ | | | | | | -591.884088 | 2.90 |
| | CCSD(T) | aug-cc-pV5Z | | | | | | -591.918156 | 2.93 |
| | CCSD(T) | CBS[c] | | | | | | -591.944934 | 2.96 |
| $Pt^+(OS)$ $^2A''$ | B3LYP | def2-TZVPPD | 2.184 | 2.067 | 1.536 | 42.2 | 305, 378, 1015 | -592.495234 | *0.58* |
| | CCSD(T) | def2-TZVPPD | 2.155 | 2.023 | 1.548 | 43.4 | 372, 430, 999 | -591.508003 | *0.49* |
| | CCSD(T) | def2-QZVPPD | | | | | | -591.628476 | *0.54* |
| | B3LYP | aug-cc-pVTZ | 2.181 | 2.053 | 1.540 | 42.5 | 318, 386, 1006 | -592.616715 | *0.56* |
| | CCSD(T) | aug-cc-pVTZ | 2.151 | 2.015 | 1.551 | 43.6 | 378, 438, 990 | -591.776966 | *0.48* |
| | CCSD(T) | aug-cc-pVQZ | | | | | | -591.865997 | *0.48* |
| | CCSD(T) | aug-cc-pV5Z | | | | | | -591.899816 | *0.49* |
| | CCSD(T) | CBS[c] | | | | | | -591.926454 | *0.49* |
| $OPtS^+$ $^2A'$ | B3LYP | def2-TZVPPD | 2.083 | 1.740 | 3.422 | 126.8 | 130, 470, 800 | -592.447115 | *1.87* |
| | CCSD(T) | def2-TZVPPD | 2.063 | 1.744 | 3.495 | 133.1 | 192, 475, 809 | -591.453520 | *1.96* |

| | | | | | | | | |
|---|---|---|---|---|---|---|---|---|
| CCSD(T) | def2-QZVPPD | | | | | | -591.573174 | *2.02* |
| B3LYP | aug-cc-pVTZ | 2.076 | 1.733 | 3.441 | 129.0 | 126, 477, 811 | -592.573743 | *1.71* |
| CCSD(T) | aug-cc-pVTZ | 2.058 | 1.733 | 3.493 | 134.1 | 121, 498, 815 | -591.732368 | *1.67* |
| CCSD(T) | aug-cc-pVQZ | | | | | | -591.815222 | *1.84* |
| CCSD(T) | aug-cc-pV5Z | | | | | | -591.847352 | *1.89* |
| CCSD(T) | CBS[c] | | | | | | -591.870220 | *2.00* |

[a] Vibrational frequencies are unscaled. [b] $Pt^+$-SO BDEs (standard font) or excitation energies (*italic font*) corrected for S.O. splitting of $Pt^+$. Uncorrected BDEs are 0.418 eV higher. [c] Complete basis set extrapolated value from X = Q and 5 results (see text).

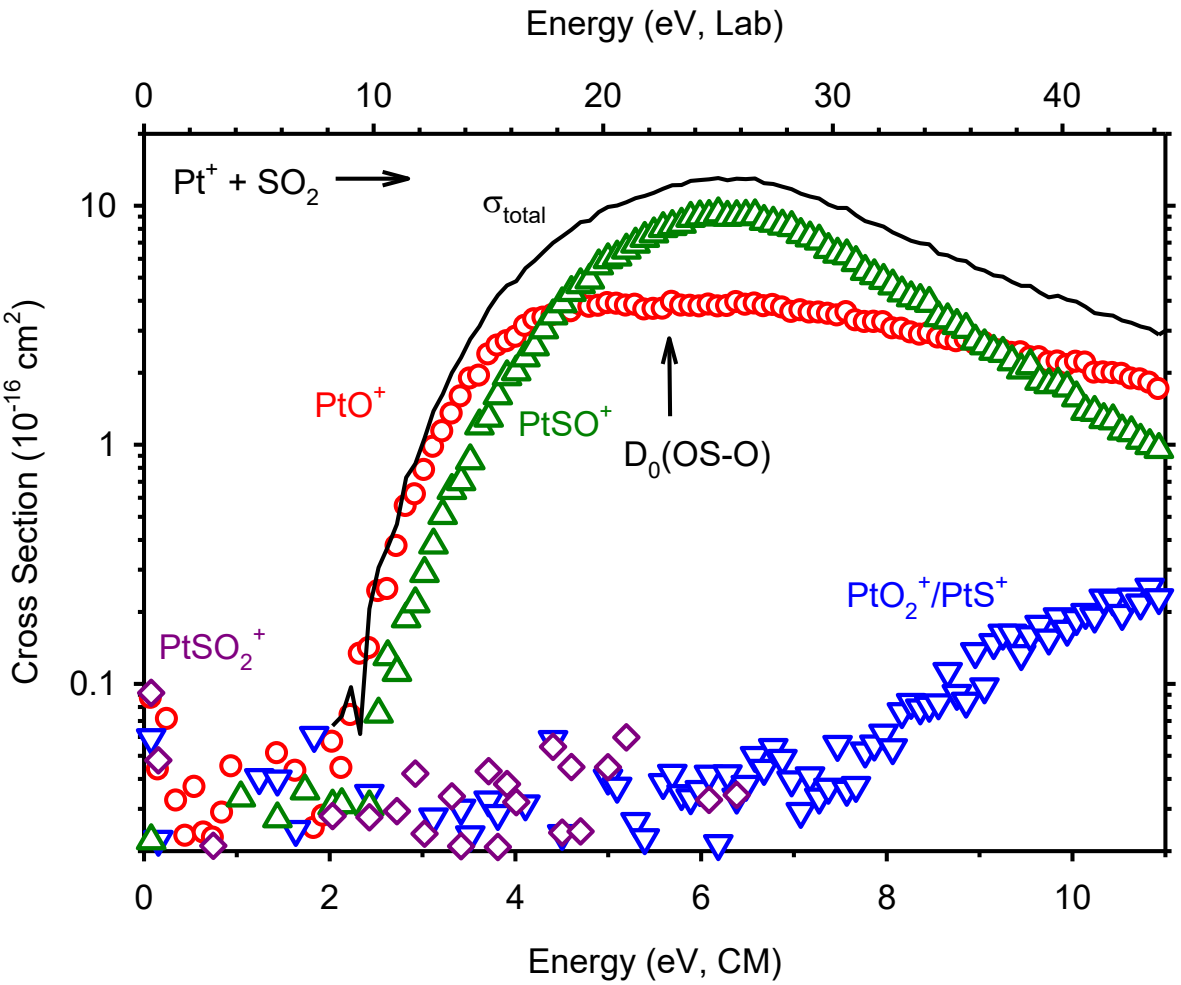


FIG. 1. Cross sections (taken at 0.16 mTorr $SO_2$ pressure) for the reactions $Pt^+ + SO_2$ as a function of the center-of-mass frame (lower axis) and laboratory frame (upper axis) kinetic energy to form $PtO^+$ (red circles), $PtSO^+$ (green triangles), $PtO_2^+/PtS^+$ (blue inverted triangles), and $PtSO_2^+$ (purple diamonds). All cross sections except that for $PtSO_2^+$ are pressure-independent. The black line represents the sum of all product cross sections (excluding $PtSO_2^+$). The vertical arrow indicates $D_0$(OS–O) at 5.66 eV.

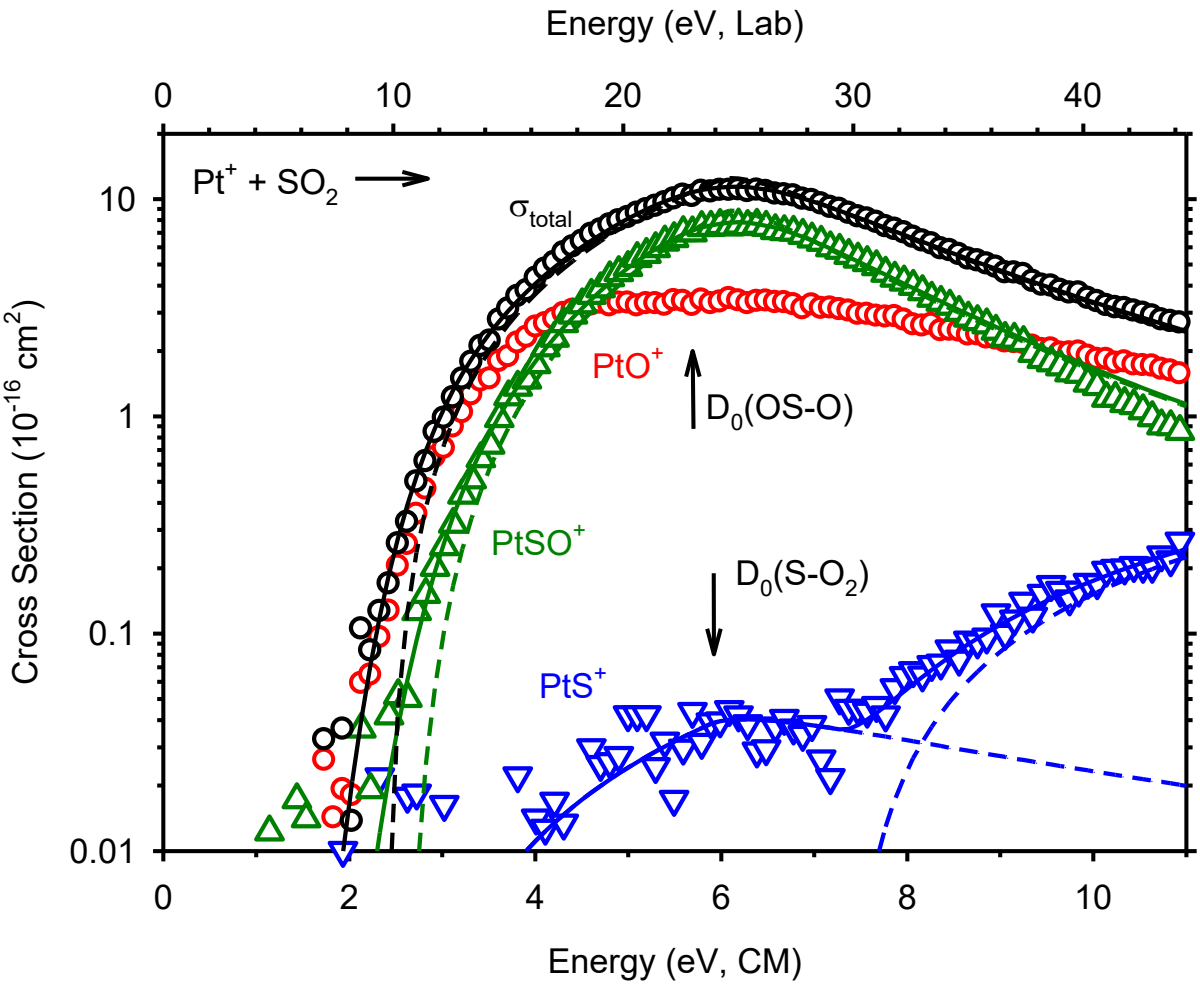


FIG. 2. Cross sections (extrapolated to zero $SO_2$ pressure) for the reactions of $Pt^+ + SO_2$ as a function of the center-of-mass frame (lower axis) and laboratory frame (upper axis) kinetic energy to form $PtO^+$ (red circles), $PtSO^+$ (green triangles), and $PtS^+$ (blue inverted triangles). Black circles represent the sum of all product cross sections. Solid lines represent the model cross sections of Eq. (1) and $P_D$ convoluted over the reactant internal and kinetic energy distributions. Dashed lines are the models in the absence of kinetic energy distributions for reactants at 0 K. Vertical arrows indicate $D_0$(OS–O) at 5.66 eV and $D_0$(S–$O_2$) at 5.90 eV.

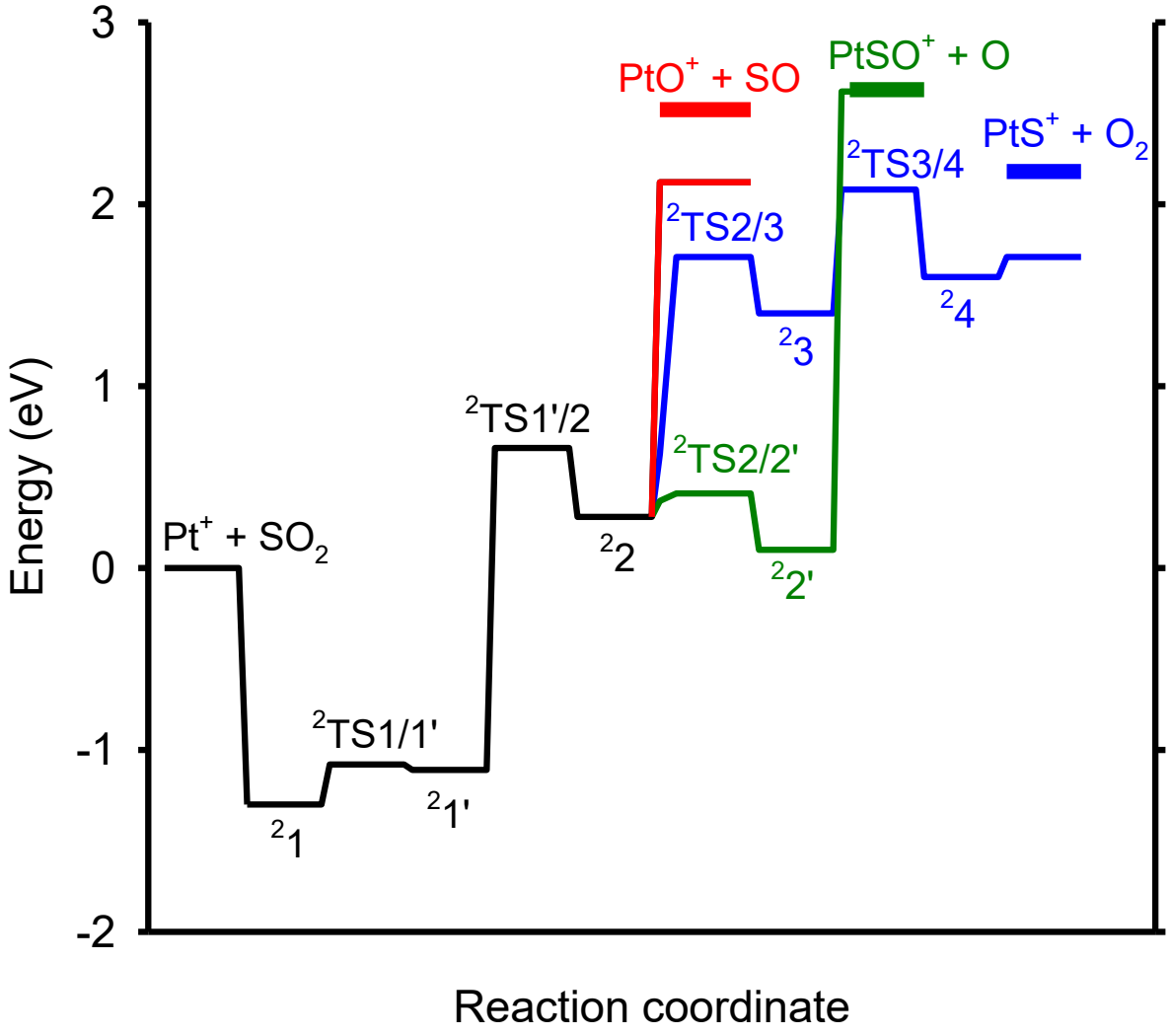


FIG. 3. Doublet spin potential energy surfaces (with S.O. corrections) for the reaction, $Pt^+$ ($^2D_{5/2}$) + $SO_2$ ($^1A_1$), calculated at the B3LYP/def2-TZVPPD level. Thick horizontal lines represent the experimental MLOC threshold energies of the products. Structures of all intermediates and transition states are shown in Fig. 4.

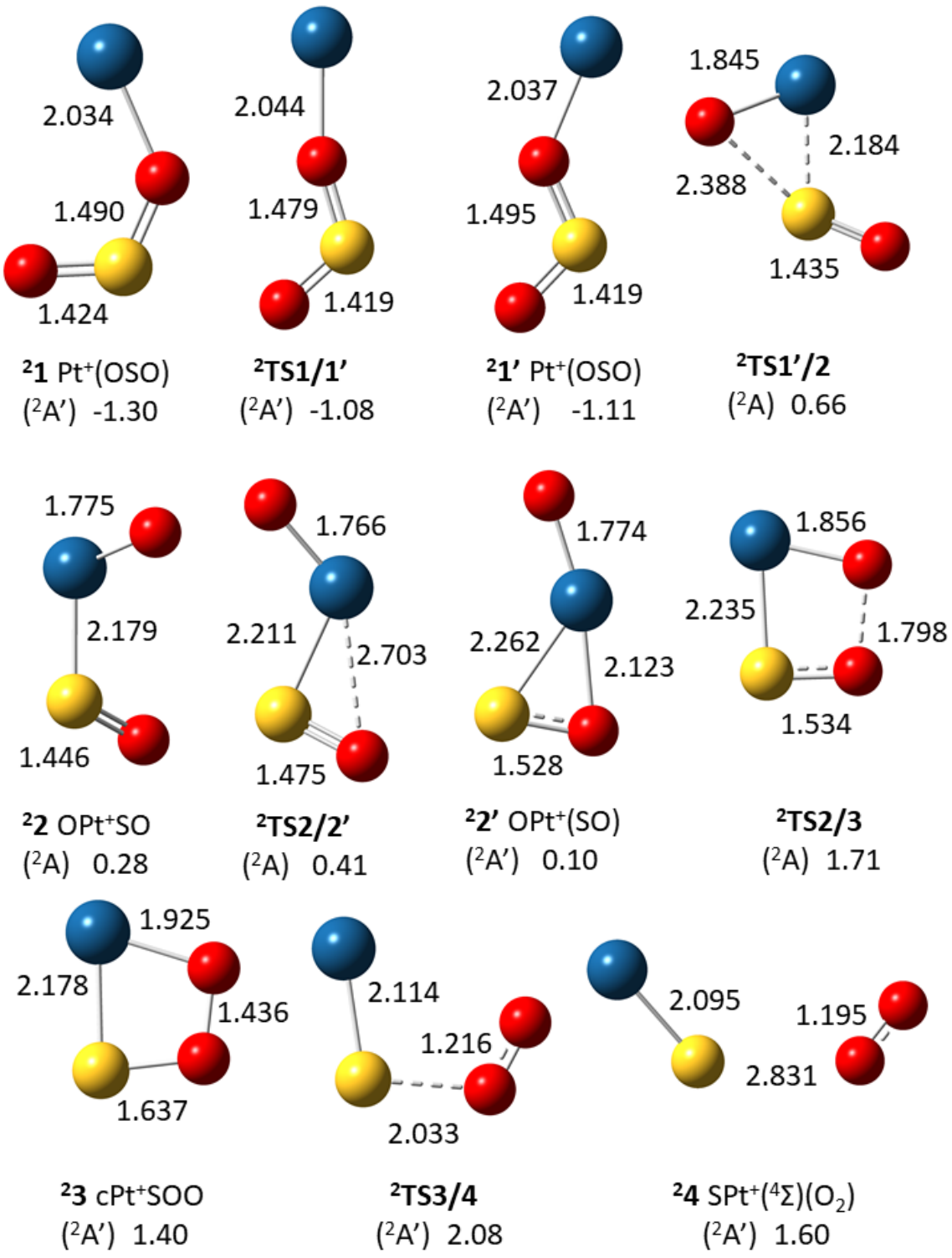


FIG. 4. Geometrical structures of doublet spin $PtSO_2^+$ intermediates and transition states in Fig. 3. These structures were optimized at B3LYP/def2-TZVPPD level. Bond lengths are indicated in Å and energies are relative to GS reactants in eV.

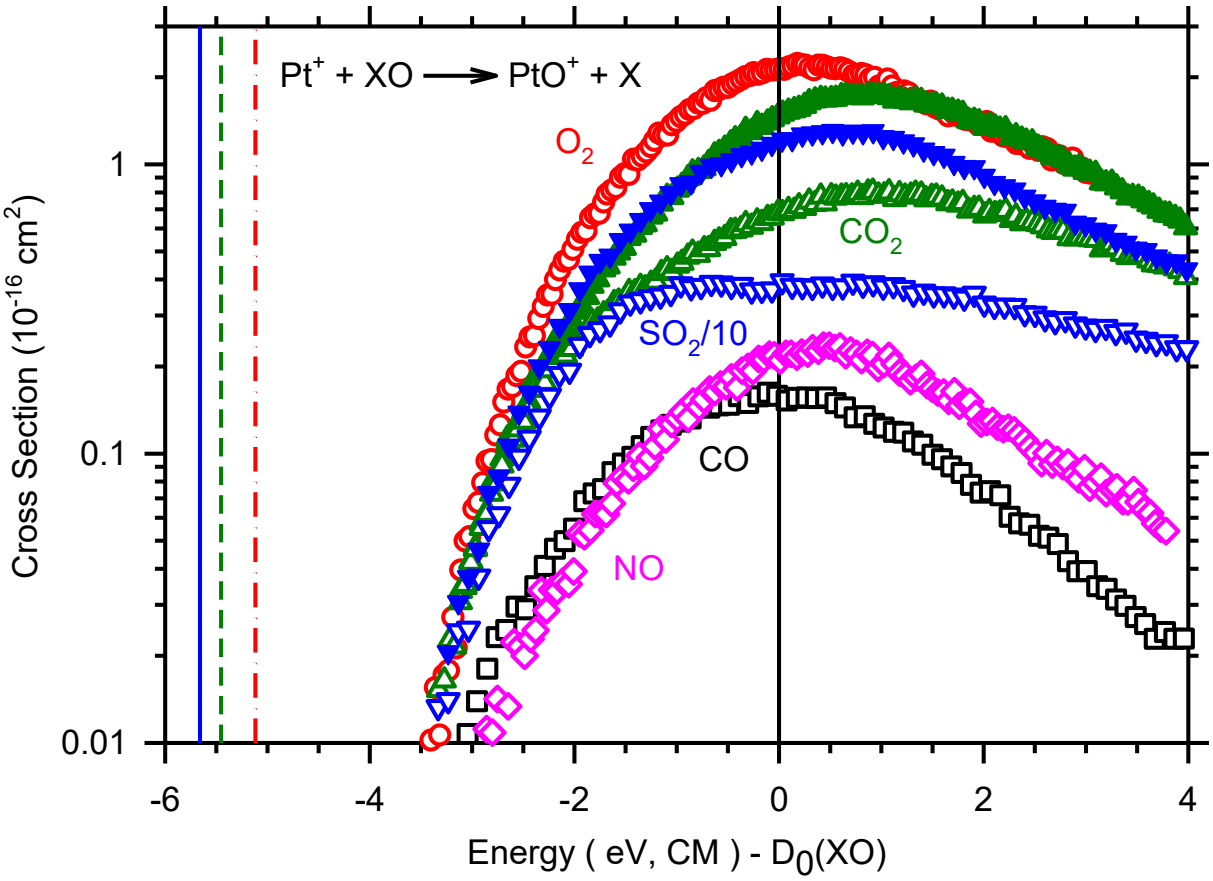


FIG. 5. Cross sections for the reactions of $SO_2$ (X = SO, blue inverted triangles, divided by 10), $O_2$ (X = O, red circles), $CO_2$ (X = CO, green triangles), CO (X = C, black squares), and NO (X = N, pink diamonds) with $Pt^+(^2D)$ as a function of the center-of-mass frame energy minus the BDE of the neutral reactant, $D_0(OS–O)$ = 5.66 eV, $D_0(O_2)$ = 5.12 eV, $D_0(OC-O)$ = 5.45 eV, $D_0(CO)$ = 11.11 eV, and $D_0(NO)$ = 6.51 eV. Open symbols show the $PtO^+$ cross section in all systems, whereas solid symbols indicate the total cross section for the $CO_2$ and $SO_2$ systems. The vertical lines indicate the zero of energy for the $SO_2$ (solid), $O_2$ (dash-dot), and $CO_2$ (dash) systems, and the 0 K BDE of the neutral XO reactant (solid) at 0 eV.